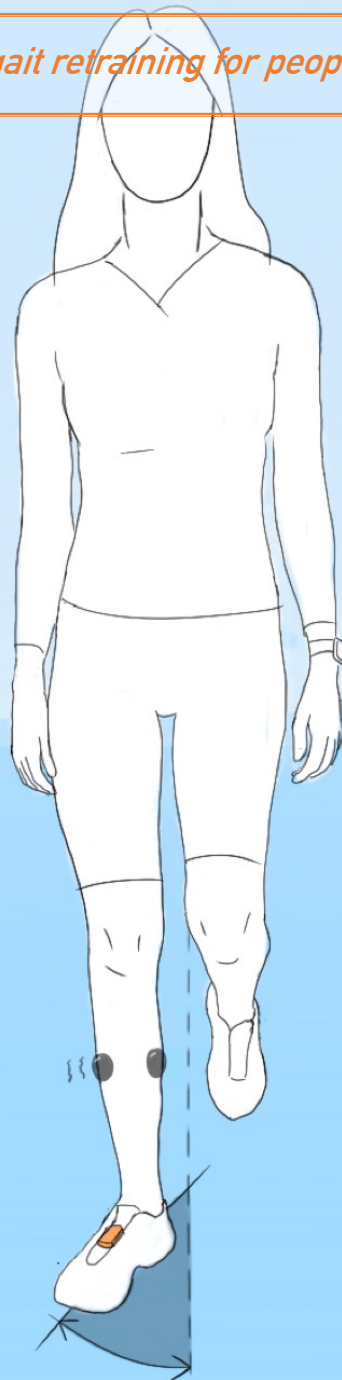


Foot Progression Angle Estimation: An Algorithm for Foot-based Single-Sensor Application

A step towards simplifying gait retraining for people with Knee Osteoarthritis



Foot Progression Angle Estimation: An Algorithm for Foot-based Single-Sensor Application

Thesis report

by

Floor Heijs

Student number: 4469046

12th September, 2023

Master thesis project (BM51035)
January 2023 - September 2023

Supervisors: Prof. Dr. Ir. J. Harlaar TU Delft
Dr. Ir. H. M. Schepers Moveshelf

An electronic version of this thesis is available at <http://repository.tudelft.nl/>.

Preface

As I conclude this graduation project, I'm reflecting on my past seven years at TU Delft. In 2015 I started my bachelor's degree in Mechanical Engineering, with the purpose of eventually beginning the master's in Biomedical Engineering. My high school years cultivated my passion for the exact subjects, and my longstanding fascination with the medical world made the Biomedical Engineering master's a perfect fit for me.

Between my master's studies, Project March crossed my path, allowing me to apply my knowledge in practice by designing walking patterns for an exoskeleton for someone with a complete spinal cord injury. This experience deepened my interest in movement analysis, rehabilitation medicine, and the integration of innovative technology in these areas. The presence of all these elements in the thesis project, Jaap introduced to me a year ago, truly fueled my enthusiasm. Now, 11 months later, I completed the project and I look back with great satisfaction. Before starting this project, I had limited experience in working with sensors, particularly IMUs, and minimal coding or research experience. I am very happy to have had the opportunity to learn more about this. This project, I admit, has been one of the most challenging so far, teaching me as much about myself as about the content.

Without the help and support of my daily supervisor, Martin, the end result would not have reached the current level. I would like to thank him for his useful insights and feedback and for introducing me to the world of movement analysis by minimal sensing. Despite his demanding schedule, he was always ready to help me. I'm also very grateful to Jaap, my supervisor from TU Delft, whose critical feedback, depth of knowledge, and motivation were instrumental. I always found our meetings enjoyable, which gave me positive energy to continue the project. Furthermore, I would like to thank the involved supervisors: Erin, Mariska and Suzanne, and all the students of the Clinical Biomechanics group for their insights, valuable knowledge, feedback and assistance during the meetings. Lastly, I would like to thank Ignazio, the co-workers and interns of Moveshelf who made me feel very welcome, I enjoyed the activities we did together and the fun moments in the office or during the daily morning meetings.

A special acknowledgement goes to the participants of my experiments. Their willingness to contribute was invaluable, and without them, this project would have remained incomplete. I'd also like to extend my gratitude to Bas and Eva for their advice in structuring the code and designing the report cover.

Above all, I'm deeply thankful to my family: my parents, sister, and brother. I am also really grateful for my roommates from the Schoonderloostraat, Vlaggenmanstraat, and Oude Delft, as well as all my other friends. Their unwavering support, encouragement, and readiness to lend an ear have been invaluable. Together, they've made the past seven years truly amazing!

Nomenclature

List of Abbreviations

F	Foot-Flat Frame
Fc	Foot-Calibration Frame
FPA	Foot Progression Angle
IMU	Inertial Measurement Unit
KAM	Knee Adduction Moment
KOA	Knee Osteoarthritis
L	Local Magnetic Earth fixed Frame
LL	Lab's Local Reference Frame
NW	Natural Walking
P	Progression Frame
PDP	Peak Deceleration Point
pKAM	Peak of KAM
S	Sensor Frame
TI	Toe-in Walking

TO Toe-out Walking

XKFCore Xsens Kalman Filter Core algorithm

ZUPT Zero Velocity Update

List of Symbols

Ω	Angular velocity
ϕ	Roll angle
ψ	Yaw angle
θ	Pitch angle
a	Acceleration
dq	Change in orientation
dv	Change in velocity
g	Gravitational acceleration
q	Quaternions
v	Velocity
v_D	Velocity drift rate

Abstract

Background: Knee Osteoarthritis (KOA) is the predominant form of osteoarthritis, and its incidence is anticipated to rise due to an ageing and increasingly overweight population. Altering the Foot Progression Angle (FPA) has demonstrated potential in mitigating the progression of KOA. Wearable feedback methods, especially those utilising single IMU sensors, have gained prominence for their cost-effectiveness, time efficiency, and potential for real-world application in FPA alteration training. This study collaboratively advances the “Knee Wear project” with the objective of designing and validating an FPA estimating algorithm during straight-line walking using the Xsens DOT sensor.

Methods: This study proposed a calibration method for sensor-to-foot orientation by developing a sensor-to-shoe fixture for consistent sensor alignment with foot direction. While static calibration remained necessary, it eliminated the need for complete sensor fixation to the shoe or dynamic calibration before each use. The fixture’s concept was verified by measuring sensor-to-shoe orientation post-fixture attachment to the shoe together with the sensor’s fixating capability on the shoe. Additionally, the difference in FPA estimation utilising the dynamic and the fixture calibration method was examined. The FPA algorithm that estimated the FPA during the mid-stance phase, utilised the orientation estimation of the Xsens DOT sensor, in combination with a heading reset to compensate for magnetic disturbances. Two FPA estimation approaches were tested: one utilising the *trajectory estimation* of the stride and another the *peak deceleration point* during the late swing phase. Experiments on 13 participants (5 males, 8 females) aimed to validate the algorithm against an optical motion capture system under three walking conditions (natural, toe-in and toe-out walking) and the efficacy of the Xsens DOT in mitigating the effects of magnetic disturbances over prolonged use.

Results: The sensor’s alignment to the foot after attachment of the fixture to the shoe provided consistency but had pronounced outliers ranging from -10° to $6,5^{\circ}$, yielding inaccurate FPA estimates utilising this calibration method. No change in the orientation of the fixture was noted during natural walking. However, fixture rotations of 1.1° externally and 0.6° internally were observed in toe-in and toe-out walking respectively. The dynamic calibration method and Peak Deceleration point algorithm yielded the most accurate FPA estimates, with mean absolute error (MAE) of less than 3.5° for all walking conditions. Notably, the FPA algorithm seemed to produce an overshooting FPA estimation, and its consistency decreased for higher FPA values. The FPA estimation over a period of 10 minutes suggested a potential minimal decline in accuracy over time, with an increase in $2,28^{\circ}$ RMSE after 10 minutes.

Conclusion: This thesis contributes to the ongoing development of wearable technologies aimed at managing KOA. By the development of an FPA estimation algorithm, evaluating multiple calibration methods, and validating its accuracy and feasibility, this study is a step towards the “Knee Wear project’s” smart-wearable feedback device, simplifying gait retraining interventions for people with KOA. While the proposed fixture calibration method needs refining for foot direction alignment, the proposed FPA algorithm, especially when combined with the dynamic calibration method, provided accurate FPA estimations. While the accuracy of the method is not absolute, the MAE magnitude of less than 3.5° is accurate enough to provide feedback on the FPA. Additional research should be done on the use of the proposed FPA estimating method by the demographic intended for the FPA feedback device.

Contents

I	Introduction	4
1	Project Introduction	5
1.1	Foot Progression Angle and its Relation to Knee Osteoarthritis	5
1.2	Foot Progression Angle Feedback Methods	6
1.3	KneeWear Project: Smart Wearable Feedback System	6
2	Background Information	8
2.1	FPA Algorithms Utilising a Single Inertial Measurement Unit	8
2.2	3D Orientation Representations	9
2.3	The Influence of Magnetic Disturbances on the Orientation Estimation	9
2.4	Different Calibration Methods of the Sensor-to-Foot Orientation.	10
3	Research Objectives	12
3.1	Gap description	12
3.2	Research Questions	12
II	Methods	14
4	Introduction to the Methods	15
5	Sensor-to-Shoe Fixture	16
5.1	Sensor-to-Shoe Fixture Design	16
6	Foot Progression Angle Estimation	20
6.1	Stance Phase Detection	20
6.2	Orientation Estimation and Transformation of the Accelerations to the Foot Frame	22
6.3	FPA Estimation	22
7	Experiment Protocol	27
7.1	Experiment 1: Fixture Orientation Following Insertion and Removal from the Shoe	28
7.2	Experiment 2: FPA Estimation Accuracy of the Algorithms for Normal, Toe-In, and Toe-Out Gait.	28
7.3	Experiment 3: Ten-Minute Walking Trial to Investigate Potential Estimation Drift.	29
8	Data Analysis	30
8.1	Data Processing	30
8.2	Sensor-to-Shoe Fixture Validation Calculations	30
8.3	FPA Estimation Algorithm Validation Calculations	31
III	Results	33
9	Orientation of the Sensor-to-Shoe Fixture to the foot	34
9.1	Sensor Alignment to the Foot After Repeated Attachments to the Shoe	34
9.2	Sensor Orientation to the Foot During the Three Walking Conditions	35
10	Validation of the FPA estimating algorithm	37
10.1	FPA Estimation by the Two Proposed Algorithms for Three Walking Conditions and Three Different Calibration Methods.	37
10.2	FPA Estimation over a Period of Ten Minutes	42

IV Closure	43
11 Discussion	44
11.1 Assessment of the Sensor-to-Shoe Fixture Concept	44
11.2 Validation of the FPA Estimation Accuracy Utilising the Xsens Dot Orientation Output.	46
11.3 Study Limitations	49
12 Recommendations	52
13 Conclusion	53
13.1 Reflect on the Research Questions	53
13.2 Closing Remarks	53
References	58
A Mid-Stance Phase detection by Jiménez et al. (2010) and Wouda et al. (2021)	59
B Sensor-to-Shoe Fixture Brainstorm Process	60
C Experiment 4: Assessing the Effect of Keeping the Fixture Inside the Shoe Across Multiple Uses	61
C.1 Introduction	61
C.2 Methods.	61
C.3 Results	62
C.4 Conclusion	62
D Additional Results	63
E FPA Estimation Box-and-Whisker plots	66
F Calibration Set-up of the Optical Motion Capture Lab	70
G Informed Consent Document	72

Part I

Introduction

Project Introduction

1.1. Foot Progression Angle and its Relation to Knee Osteoarthritis

Worldwide, nearly a quarter (22.9%) of individuals over 40 years of age suffer from Knee Osteoarthritis (KOA). Given that osteoarthritis worsens with weight gain and ageing, an increasingly older and heavier population suggests that the prevalence of KOA will continue to rise [1, 2]. At the structural level, KOA is characterised by the degeneration of cartilage in the knee joint, which is marked to be incurable. Patients with KOA, are experiencing chronic pain in the knees, reduction in muscle strength and range of motion, and a decrease in the quality of life [3, 4], which all contribute to a decline in overall health and well-being. Currently, KOA is managed with analgesics, and when these prove to be insufficient, lead to the consideration of a total knee replacement. However, this procedure is expensive, intricate, and may not guarantee complete effectiveness [5]. As a result, the focus is currently on preventing or slowing down the cartilage degeneration process in early-stage KOA, to delay the need for surgery [6].

It is important to note that the etiology of osteoarthritis is complex and not the same for every individual. However, disruption of cartilage metabolism including inflammation, and mechanical overload are two important factors. In this thesis, the focus is specifically on the mechanical overload aspect as a potential contributor to osteoarthritis. One potential intervention for this involves implementing gait modification strategies aimed at reducing knee joint loading, with the expectation of reducing degeneration of cartilage [7]. It has been shown that the Knee Adduction Moment (KAM) serves as an externally measurable proxy for the internal knee load, that relates to the progression of KOA [8, 9]. Due to higher compressive forces on the cartilage, the medial compartment of the knee joint is more susceptible to osteoarthritis compared to the lateral compartment [7, 10, 11]. The KAM contains two peaks during gait, the first peak of KAM (1st pKAM) occurs during the early stance phase, where body weight is transferred to the limb and results in an increase of the loading on the knee joint. The second peak of KAM (2nd pKAM) occurs during the late stance phase due to the push-off of the foot which leads to increased loading on the leg and, therefore, on the knee joint. KAM impulse represents the area under the KAM curve during a gait cycle, representing a measure of the magnitude and duration of the knee adduction loading.

Three systematic reviews have shown that altering the Foot Progression Angle (FPA) is an effective strategy for reducing KAM [12, 13, 14]. The FPA is defined as the angle between the line from the heel to the second metatarsal head and the line of the walking direction. FPA gait modification strategy was not only effective in lowering KAM but additionally has been reported by participants to be a feasible and comfortable gait modification [15, 16, 17, 18]. This finding was supported by Caldwell et al. (2013) [19], who demonstrated that FPA modification reduced KAM, while it was also the least demanding in terms of increased energy expenditure and perceived work-load when compared to strategies such as trunk lean and medial weight shift of the foot. However, it should be noted that a difference has been reported between healthy individuals and those with KOA in their capability to alter the FPA [20, 21], as well as in the reduction of KAM resulting from these alterations [14, 13]. Given the relation of KAM to the knee joint loading and the influence of FPA on its reduction, using FPA as a surrogate measure provides a feasible approach for feedback methods targeting a decrease in knee loading.

Gait modification strategies, aimed at altering the FPA, have shown promise in reducing knee joint

loading and mitigating the progression of KOA [12, 13, 14]. To effectively implement such strategies, providing feedback to individuals during gait adaptation plays a crucial role. Feedback serves as an essential tool in the motor learning process, helping individuals acquire new motor skills and maintain consistency in gait alterations.

One of the primary advantages of feedback is its ability to facilitate real-time awareness of gait patterns. Through visual or haptic cues, individuals can receive immediate information about their FPA during walking. This allows them to make instant adjustments and reinforces the desired gait pattern [22, 23]. By continuously monitoring their FPA, individuals can better execute the modifications needed to achieve the desired gait modifications. As a result, the motor learning process becomes more efficient, and the likelihood of successful and sustained FPA alteration increases [24].

1.2. Foot Progression Angle Feedback Methods

Different feedback methods are used to train the FPA alterations during gait, with the most commonly used being visual feedback. Often, this feedback method is dependent on a laboratory because the estimation of the FPA is done by an optical motion capture system, and the feedback is provided on a screen in the lab. Typically, this method necessitates a laboratory setting, as FPA estimation relies on an optical motion capture system and feedback is displayed on an in-lab screen. Such methods are integrated into training programmes where participants undergo several weeks of FPA training, aiming to embed the altered FPA into their daily walking patterns. Yet, post-training observations revealed that the modified FPA diminishes over time, subsequently resulting in less reduction in KAM [24]. This indicates that motor learning of the alteration of the FPA of the individuals may take more time, or will not occur at all. Moreover, in-lab training programs, due to their reliance on motion capture systems, are very time-consuming and expensive.

Alternative feedback methods are wearable (laboratory-independent) feedback methods such as virtual reality feedback and haptic feedback where inertial measurement units (IMUs) are used to measure a person's gait pattern. Wearable feedback methods provide better FPA alteration than the non-wearable ones (laboratory-dependent), but also they are less expensive and time-consuming due to the use of IMUs instead of the Motion Capture System [25, 26]. In addition, with these wearable FPA feedback systems, the participants can ultimately train their FPA alteration in their daily life, which will maintain consistency in the alteration. All the above-described advantages increased the interest in the development of wearable feedback methods that can be utilised in the home environment [26, 27, 25, 28].

1.3. KneeWear Project: Smart Wearable Feedback System

The KneeWear project is an R&D cooperation between the two companies Moveshelf and Elitac Wearables, within the framework of the SME Innovation Stimulus Region and Topsectors (MIT) scheme, supported by the Province of Utrecht. The project aims to develop a smart wearable with haptic feedback combined with a digital platform for people with KOA. The smart wearable haptic feedback device will provide (semi-)real-time information about the FPA and intuitively feed this back to the user through positioned vibrations. Additionally, the information about the FPA will also be converted to the digital platform, and feedback on the (long-term) progress of the FPA can be shared with the specialist in the hospitals and clinics as well as the user improving the consistency of the FPA alteration [29]. Patients can perform gait training at home, while the care (analysis) is performed from distance by the specialist. This can prevent a significant number of hospital or clinic visits and thus significantly reduce healthcare costs.

The proposed working principle of the smart wearable haptic feedback device is illustrated in figure 1.1. An Xsens DOT inertial sensor [30] is used and connected through Bluetooth to the phone of the user. On this phone the "MoveshelfMobile" and Elitac applications are located, the MoveshelfMobile application connects to the Moveshelf platform of the physician, while the Elitac application connects through Bluetooth to the vibration motors.

The Moveshelf application currently incorporates a proof-of-concept FPA estimating algorithm. This algorithm translates IMU data into the user's FPA at each step. If the FPA exceeds set thresholds, information is relayed to the Elitac application, which then signals the vibration motors. Although the monitoring platform remains in development, decisions regarding the display of monitoring data and the choice of feedback parameters within the device are pending. The next pivotal step in the project entails

integrating a validated FPA estimating algorithm into the Moveshelf application.

The FPA is defined as the angle between the foot's orientation and the walking direction, making this relationship particularly consequential when walking directions change. For example, during a turn, the walking direction diverges significantly from straight-line walking, resulting in extreme FPA values that are unrepresentative and unsuitable for feedback. For this reason, estimating FPA will be only relevant during straight-line walking. The focus of this thesis lies on the design and validation of an FPA estimating algorithm during straight-line walking.

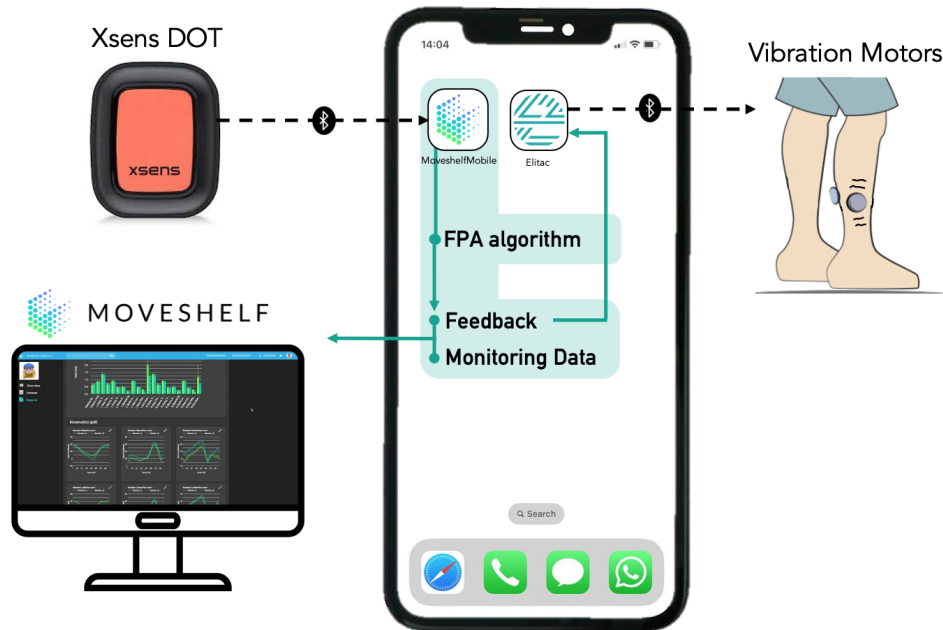


Figure 1.1: Overview of the working principle of the smart FPA feedback system of Moveshelf and Elitac. The main focus of this thesis project lies on the FPA algorithm

Background Information

2.1. FPA Algorithms Utilising a Single Inertial Measurement Unit

The objective of this section is to examine and contrast the methodologies of three published papers that proposed algorithms for FPA estimation using a single Inertial Measurement Unit (IMU). Traditionally, estimating the FPA during walking has predominantly employed optical motion capture systems. This method entails placing reflective markers on the subject's foot and tracking their trajectories using optical motion capture cameras. Given the system's high expense and its restriction to specific labs, alternative techniques are increasingly explored. Consequently, an increased interest is noticed in employing IMUs on the foot, coupled with algorithms, to estimate the FPA.

Three published papers by Huang et al. (2016) [31], Tan et al. (2021) [32], and Wouda et al. (2021) [33] proposed algorithms for FPA estimation using a single IMU positioned on the dorsal side of the foot. These algorithms share a similar working principle. Initially, the IMU undergoes calibration to align its measurements with the participant's physical foot frame. Subsequently, the (mid-)stance phase is detected to extract relevant data for accurate foot orientation estimation. Finally, the walking direction is determined to calculate the FPA, defined as the angle between the foot orientation and the walking direction within the horizontal plane.

IMU drift, caused by sensor noise and bias, can lead to errors in orientation estimation. To address this, sensor fusion techniques such as Kalman filters or complementary filters are employed to reduce drift and improve IMU accuracy. However, complete elimination of drift remains challenging over extended time periods.

The working principles of the proposed algorithms of each paper are outlined below.

2.1.1. Huang et. al. (2016) FPA Estimating Algorithm

Huang et al. (2016) [31] used a magnetometer-based approach, combining static and dynamic calibration methods to establish the sensor's orientation in the anatomical foot frame [34]. The static calibration involved standing still for 5 seconds to measure gravitational accelerations, determining the z-axis of the foot. Dynamic calibration used dorsiflexion and plantarflexion of the ankle to find the y-axis using Principle Component Analysis (PCA) [35]. The x-axis was obtained by applying the right-hand rule to the previously defined axes, with the y-axis redefined to ensure perpendicularity to the z-axis.

Stance phase detection employed a zero-velocity algorithm with acceleration and gyroscope data [36], approximating the stance duration as 60% of the stride time using detected heel strike events. Quaternion data from the gyroscope was integrated to obtain foot orientation, and corrected for drift with accelerometer and magnetometer data using a gradient descent algorithm. Foot trajectory estimation involved double integrating accelerations, corrected for drift with zero velocity updates (ZUPT) [37]. The walking direction was estimated using a complementary filter applied to the foot trajectory at each previous stride. Lastly, the FPA was calculated as the average angle between the foot vector and walking direction, projected onto the horizontal plane, over the entire stance phase.

2.1.2. Wouda et. al (2021) FPA Estimating Algorithm

Wouda et al. (2021) [33] proposed a magnetometer-free algorithm for FPA estimation, having similarities to Huang et al.'s approach [31]. The calibration method for sensor-to-foot orientation was the same, but

stance phase detection differed. Only the mid-stance phase was detected using an alternative zero velocity detection approach [38]. Foot orientation was determined by integrating gyroscope angular velocities during each mid-stance phase, corrected for potential drift with a Zero Angular Velocity Update (ZAVU).

Trajectory estimation of the foot was performed by double integrating the accelerations in the foot frame, performing a Zero-Velocity-Update (ZUPT) to compensate for integration drift. The FPA was calculated as the angle between the foot direction at the beginning of the stride and the walking direction from the beginning to the end of the stride.

2.1.3. Tan et al. (2021) FPA Estimating Algorithm

Tan et al. (2021) [32] proposed also a magnetometer-free algorithm, where the calibration method was performed differently than the previously discussed papers. The sensor was placed in a fixated location in the shoe, eliminating the need for a calibration method performed by the participants, as the orientation of the sensor to the foot was known beforehand. The stance phase was detected by a gait event detecting algorithm [39].

The algorithm also integrated angular velocities to the orientation of the foot at each stance phase, where a gradient descent algorithm is used to correct for drift. The gradient descent algorithm is the same as Huang et al. (2016)[31] but used no magnetometer data, only accelerometer data is used for correction. The FPA is then calculated in a different manner than the one of Wouda et al. [33] and Huang et al. [31].

Instead of trajectory estimation, the walking direction was estimated under the assumption that all accelerations perpendicular to the walking direction were zero. A 'current step frame (C-frame)' was defined, aligning the y-axis with the walking direction. The FPA was then obtained by calculating the accelerations in the C-frame through a rotation matrix of the foot frame to the current step frame, setting the accelerations in the x-direction to zero (equation 6.12 and 6.13). The accelerations from the peak deceleration point during the second half of the swing phase in the foot-flat frame were used.

2.2. 3D Orientation Representations

Three-dimensional orientation can be represented in three different ways: Euler angles, Quaternions, and Rotation matrices. Euler angles define orientations through three distinct angles in a certain order: roll (Φ), pitch (Θ), and yaw (Ψ). While they offer an intuitive approach, they are susceptible to gimbal lock, leading to potential loss of a degree of freedom and ambiguities, particularly at pitch angles near 90 degrees [40]. Quaternions on the other hand, are composed of one real part (q_0) and three imaginary components ($q_1i + q_2j + q_3k$), provide computational efficiency and stability in 3D rotations. Rotation Matrices, 3x3 matrices built from directional cosines that represent angles between a vector and coordinate axes, also serve as robust orientation descriptors without the singularity issues of Euler angles.

The Xsens DOT sensor, which is to be used as the IMU sensor of the haptic feedback device (Section 1.3), utilizes quaternions in its orientation output, describe the sensor orientation (S) relative to the Local Earth-Fixed Reference Frame (L), which is defined as a right-handed Cartesian coordinate system with Y positive to the North. These quaternions can be transformed into the rotation matrix (R_S^L) characterising the sensor's unit vector expressed in the local earth magnetic reference frame:

$$R_S^L = \begin{bmatrix} 2(q_0^2 + q_1^2) - 1 & 2(q_1q_2 - q_0q_3) & 2(q_1q_3 + q_0q_2) \\ 2(q_1q_2 + q_0q_3) & 2(q_0^2 + q_2^2) - 1 & 2(q_2q_3 - q_0q_1) \\ 2(q_1q_3 - q_0q_2) & 2(q_2q_3 + q_0q_1) & 2(q_0^2 + q_3^2) - 1 \end{bmatrix} \quad (2.1)$$

2.3. The Influence of Magnetic Disturbances on the Orientation Estimation

The quaternions from the Xsens DOT are corrected for drift employing a built-in Xsens Kalman Core algorithm (XKFCore) utilising accelerometer and magnetometer data. However, magnetic disturbances from nearby electrical devices, metal structures, or wiring could affect the magnetometer readings, thereby potentially degrading the accuracy of orientation estimates [41, 42, 43]. These disturbances are particularly relevant when the sensor is worn close to the ground, such as in the intended foot placement application, as described by de Vries et al. (2008) [44].

Considering the specific use case of the FPA haptic feedback device, which might involve both indoor (e.g., physiotherapist's clinic) and outdoor (e.g., urban or rural areas) environments, these magnetic disturbances could become a considerable challenge. Tan et al. (2021)[32] and Wouda et al. (2021)[33] introduced magnetometer-free FPA estimating algorithms, but these tend to be less accurate than those using magnetometers for drift compensation [31]. A promising strategy for the mitigation of the magnetic disturbances, detailed in Chapter 6 Section 6.2, involves a heading reset during the gait cycle's stance phase. This reset procedure allows the orientation to be realigned periodically, reducing the impact of magnetic disturbances on the Orientation estimation. One should note that magnetic disturbances can still exert an effect on the change in orientation (dq) output values for the rest of the step, which can lead to drift.

While magnetic disturbances are a significant concern for IMU-based orientation estimates, the combination of quaternion representations (which avoid gimbal lock) and strategic heading resets during the stance phase (which help to mitigate the effects of magnetic disturbances) might enable accurate and reliable FPA estimation using the Xsens DOT sensor.

2.4. Different Calibration Methods of the Sensor-to-Foot Orientation

As discussed before in section 2.1 two different calibration methods are utilised in the previous papers validating an FPA estimating algorithm using a single IMU on the foot. The calibration method for the sensor is crucial in determining the accurate orientation of the sensor relative to the foot. This accuracy is essential as it allows for the transformation of sensor-measured accelerations, angular velocities, and orientations into foot-represented values. An inaccurate definition of this relative sensor orientation can lead to inaccuracies in the determination of the FPA. The calibration process establishes the foot's local reference frame (see Figure 2.1), where the resulting rotation matrix ($R_{F_c^S}$) can translate, for example, the sensor's accelerations, in the sensor frame (S), into accelerations described in the anatomical foot calibration frame (F_c).

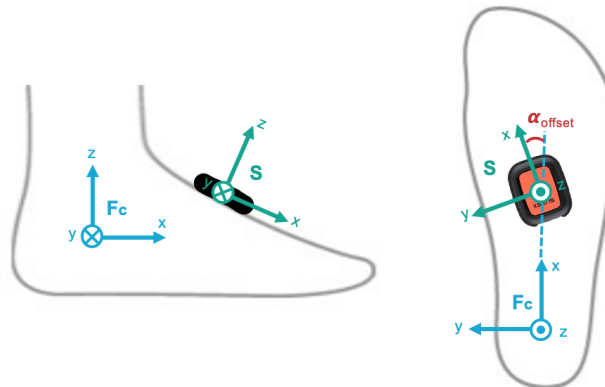


Figure 2.1: The sensor frame (S) orientation in comparison to the anatomical foot calibration frame (F_c) orientation.

Embedding the sensor at a fixed shoe location, as conducted by Tan et al. (2021)[32], eliminates the need for pre-use calibration, but restricts the user to a single pair of shoes and increases device cost. Methods like Huang et al. (2016)[31] and Wouda et al. (2021)[33], where the IMU is fixated between shoelaces, allow for the use of personal shoes. However, this limits the user to lace-up shoes, and the sensor can shift during use because of improper fixation, compromising the FPA accuracy (figure 2.2). Next to this is the calibration method not only time-consuming but also may not be the most accurate way to determine the rotation axis, as the user should genuinely rotate their feet around the 'hinge' ankle axis and should not incorporate any endo- or exorotation during the dorsi- and plantarflexion task ('dynamic calibration').

*IMU fixated between
shoe laces*



- Advantage:**
- + The user can use the device with his own shoes
 - + Cheaper
- Disadvantage:**
- The calibration method must be done prior to each use because the orientation of the sensor is unknown. → Not user friendly
 - Sensor is not well fixated

*IMU in fixated in
shoe sole*



- Advantage:**
- + The calibration method is not needed → User-friendly
- Disadvantage:**
- The user has to always wear a manufactured shoe when using the feedback device → Expensive and not user friendly

Figure 2.2: Overview of the different IMU placements on the shoe among previous methods, and their corresponding advantages and disadvantages

In the context of the KneeWear Project (section 1.3), where permanently fixating the sensor in a shoe and performing constant re-calibration before every use are both impractical, a novel hybrid approach has been preferred. This approach involves the development of a sensor-to-shoe fixture that can be attached to any shoe type, providing a partially predetermined sensor-to-shoe orientation. By ensuring that the fixture maintains consistent axis alignment with each use, only one additional axis, i.e. the z-axis, requires static calibration. Notably, this hybrid approach eliminates the need for dynamic calibration or permanent sensor placement, addressing the challenges of impracticality and enhancing the overall usability of the device.

Research Objectives

3.1. Gap description

Different calibration methods are proposed in previous literature. Within the context of the KneeWear project, permanently affixing the sensor inside the shoe is not optimal due to high manufacturing costs and the limitation of binding each user to a single shoe. Additionally, dynamic calibration methods appear impractical and potentially inaccurate, given the required plantar-dorsiflexion task before each usage. This thesis aims to devise a sensor-to-shoe fixture that consistently aligns the sensor with the foot's direction each time it is attached to the shoe, which eliminates the use of the dynamic calibration method. It is essential to validate the fixture's performance in terms of sensor attachment and alignment following multiple uses. Furthermore, an unaddressed difference exists between the FPA estimation accuracies utilising the dynamic and the proposed sensor-to-shoe fixture calibration methods.

Three previous papers validated FPA estimating algorithms utilising a single sensor on the foot. One study utilised magnetometer data to correct orientation drift [31]. Nevertheless, when the IMU is placed on the foot near the ground, it becomes vulnerable to magnetic disturbances from for example sources like iron objects or electrical devices, potentially affecting FPA accuracy [44]. Two recent alternative studies introduced magnetometer-free FPA algorithms, integrating raw gyroscope data from the IMU for orientation estimation [32, 33]. However, under uniform magnetic fields, these algorithms proved less accurate than those employing magnetometer drift compensation.

The hypothesis is that utilising the Xsens DOT's orientation output, a fusion of gyroscope data corrected for drift by the XKFCore algorithm combining both magnetometer and accelerometer data, will result in higher FPA estimation accuracy than integrating raw gyroscope data. Moreover, initiating a heading reset at the onset of each step is proposed to significantly mitigate the influence of magnetic disturbances. It remains to be seen whether this hypothesis holds and to what degree the FPA accuracy varies between trajectory estimation and peak deceleration point assessment. Understanding the impact of these different approaches on FPA estimation accuracy will contribute to identifying the most reliable and accurate method.

The long-term effects of magnetic disturbances on orientation estimates over time need to be explored. Performing the heading reset will discard the influence of magnetic disturbances over time, however, in long-term exposure scenarios, the efficacy of the XKFCore filter may decline. Therefore, it is necessary to investigate whether magnetic disturbances affect the accuracy of orientation estimation using the Xsens DOT, particularly in long-term exposure scenarios.

3.2. Research Questions

Following the gap description, this study aims to address two primary areas of investigation: the efficacy of the sensor-to-shoe fixture calibration method, and the accuracy of the FPA estimating algorithm. The following research questions have been formulated:

Sensor-to-Shoe Fixture Calibration Method

Research Question 1

How effective is the sensor-to-shoe fixture as a calibration method for an FPA estimating algorithm?

Sub-questions:

- Does the sensor-to-shoe fixture maintain consistent sensor alignment with the foot direction through repeated attachments and detachments?
- How effectively does the fixture stabilize the sensor's attachment to the foot during walking?
- What is the FPA estimation accuracy difference between the dynamic and fixture calibration methods?

FPA Estimating Algorithm

Research Question 2

How accurate is the FPA estimating algorithm utilising the Xsens DOT orientation output compared to an optical motion capture system?

Sub-questions:

- What is the FPA estimation accuracy with the Xsens DOT orientation output compared to an optical motion capture system?
- How do magnetic disturbances influence the FPA estimation accuracy over 10 minutes?
- What is the estimation accuracy difference in the FPA estimation between trajectory estimation and peak deceleration point algorithms?

Part II

Methods

Introduction to the Methods

The FPA estimation out of a single Xsens DOT Sensor on the foot and its output values involves six primary components, as shown in figure 4.1. Notably, the FPA is only relevant during the stance phase, and therefore the mid-stance phase is detected by a zero-velocity approach [38] by the change in velocity (dv) and change in orientation (dq) outputs of the Xsens DOT Sensor. The foot orientation at each step is obtained by the Xsens DOT output orientation (quaternions), which, once converted to a rotation matrix, is multiplied with the sensor-to-foot orientation (R_{Fc}^S) obtained by the dynamic or fixture calibration method, to rotate the sensor's-measured accelerations to the foot-flat (F) frame throughout each step. Subsequently, these accelerations facilitate the computation of FPA for two different methods. The first method, based on Tan et al. (2021) [32], determines the FPA for each step out of the accelerations during the peak foot deceleration point during the second half of the swing phase. The second method, based on Wouda et al. (2021) [33], employs strap down-integration to determine the trajectory, after which the FPA is calculated using the angle between the foot vector and the step's heading vector.

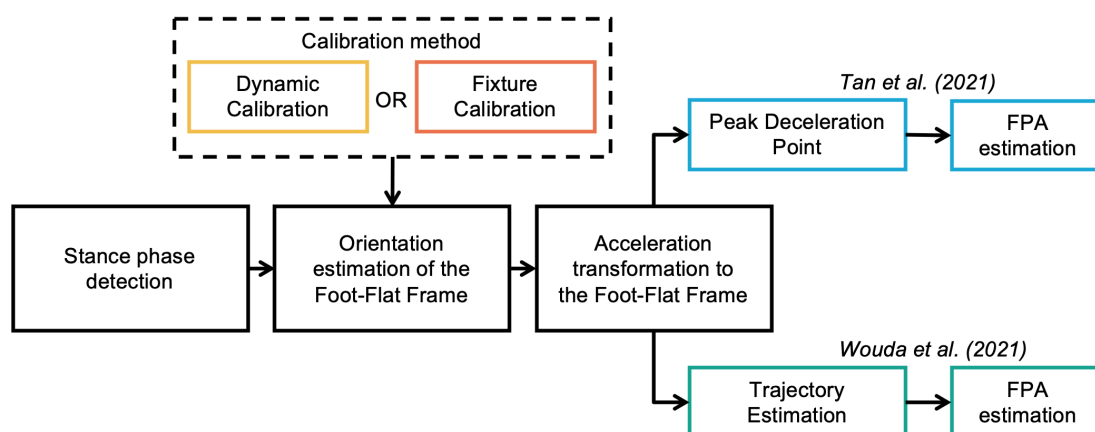


Figure 4.1: Flow chart detailing the six primary components for the FPA estimation methodology. The first four components include the Calibration Method, Stance Phase Detection, Orientation Estimation, and Transformation of Accelerations to the Foot-Flat Frame, establishing the data processing steps. The final two components, Peak Deceleration Point and Trajectory Estimation represent two different methods for estimating the FPA.

As previously mentioned (Chapter 3), this thesis has dual objectives: first, to validate the FPA estimating algorithm, and second, to develop a sensor-to-shoe fixture that aligns the sensor with a specific axis of the foot. To this end, the methodology section includes four chapters. The first focuses on the design of the sensor-to-shoe fixture and its accompanying calibration approach. The second elaborates on the working principles behind the FPA estimation algorithm. The third chapter outlines the experimental protocol used to validate both the fixture concept and the algorithm. The final chapter discusses data analysis.

Sensor-to-Shoe Fixture

5.1. Sensor-to-Shoe Fixture Design

In the context of the KneeWear Project (section 1.3), where permanently fixating the sensor in a shoe and constant re-calibration before every use are both impractical, a hybrid approach is preferred. This involves designing a sensor-to-shoe fixture that attaches to any shoe type, with a partially predetermined sensor-to-shoe orientation. If the fixture maintains a consistent axis alignment each time it's used, only one additional axis (the z-axis) requires static calibration to ultimately determine the rotation matrix ($R_{F_c}^S$) describing the sensor's orientation in relation to the foot's anatomical structure, where F_c denotes the foot calibration frame.

5.1.1. Requirements and Wishes

The preferred location for the IMU is the dorsal side of the shoe, as it is the location where the probability of impact or disruption during the user's movements is the least [45]. Additionally, the fixture must not affect the user's walking pattern, so it must be lightweight, not increase the chance of slipping, not decrease the range of freedom, and not cause pain or discomfort to the user. It must maintain a consistent sensor direction along one axis of the foot's coordinate system. As seen in figure 2.1, from the top view of the foot, the sensor can be angled relative to the direction of the foot (x-axis of the foot calibration frame), as long as the 'alpha' offset is always the same. Additionally, the goal is a fixture that fits any shoe and is easy to attach and remove.

		Reason
Requirements	Must maintain a consistent sensor direction along one axis of the foot's coordinate system. (max range of ± 1 degrees around the z-axis)	Necessary for a robust calibration method
	Must not increase the risk of slipping	Must not affect any of the user's walking patterns
	Must be lightweight (maximum of 0.2 kg)	Must not affect any of the user's walking patterns
	Must not decrease the range of freedom	Must not affect any of the user's walking patterns
	Must not cause pain or discomfort	User-friendly and must not affect any of the user's walking patterns
Wishes	Should fit in any type of shoe and any foot size	User-friendly
	Should be aesthetically pleasing	User-friendly

Table 5.1: List of requirements and wishes for the sensor-to-shoe fixture concept to establish a hybrid method for the calibration of the sensor to the shoe orientation.



Figure 5.1: Sock Concept, for the sensor-to-shoe fixture with the fixation band open, front and side view respectively.



Figure 5.2: Sock Concept, for the sensor-to-shoe fixture with the fixation band open, side and front view respectively.

5.1.2. Prototyping

A brainstorm session for the design of the sensor-to-shoe fixture was conducted in which several concepts were created and tested. An overview of these can be found in appendix B. In collaboration with Elitac Wearables, a mock-up session produced a sock concept (Figure 5.1 and 5.2), accommodating all shoe types. The sock design incorporated an elastic fabric stretching from the metatarsal region to the ankle and distal tibia. On the dorsal side of the sock, a non-flexible stud is mounted which runs the entire length of the sock, ensuring that the sensor is always pointing in the same forward direction. On top of this, the sensor holder of Movella is attached where the Xsens DOT can be clicked in and out. Anti-slip plastic was secured under the metatarsal region of the fabric, ensuring the shoe maintains its grip. An extra fixation strap was connected to the anti-slip compartment, providing enhanced sensor stability during walking.

Preliminary pilot studies indicated that the sock's elastic fabric was prone to overstretching due to repetitive application and removal, resulting in fixture function degradation. As a result, a new concept was created, abandoning the desire to adapt the fixture to any shoe type. This new concept featured a patch intended to be placed on the shoe tongue. The patch was designed to be as large as possible in both length and width. Increasing the length improved the potential for alignment in one direction while expanding the width enhanced the chance of correct fixation. The patch was designed for insertion and removal between the shoe tongue and laces.



Figure 5.3: (1) Placing the sensor-to-shoe fixture on top of the shoe tongue underneath the laces. (2) Tighten the shoelaces for fixation of the shoe and the sensor-to-shoe fixture. (3) Fixture with the sensor fixated on the shoe.

5.1.3. Final Prototype

The final concept incorporated a two-layer soft leather patch, stitched together, with a Movella sensor holder positioned at the centre. This Movella sensor holder allows for replacement of the sensor, in between uses. The patch was designed to be placed on the shoe tongue underneath the laces (Figure 5.4 and 5.3). After lacing the shoe, the patch is assumed to be secured between the shoe tongue and the laces, ensuring reliable fixation and accommodating different shoe widths. This design allowed for easy attachment and removal of the sensor-to-shoe fixture, making it suitable for various shoe types with shoe laces. In addition to being able to place the sensor-to-shoe fixture on the shoe tongue for each use, it could also remain in the shoe between uses. Where after putting the shoe on, the fixture might require minor directional adjustment.



Figure 5.4: The sensor-to-shoe fixture: a patch of soft leather with an Movella DOT holder centred

5.1.4. Final calibration method with the sensor-to-shoe fixture concept

The final calibration method for the sensor-to-shoe fixture can be determined using a stepwise process. Firstly, a static calibration is performed by measuring the mean accelerations (a_x , a_y and a_z) while the foot is stationary for 5 seconds. This provides the gravitational acceleration $g = \sqrt{a_x^2 + a_y^2 + a_z^2}$, which aligns the z-axis of the F_c frame. The relationship between the sensor (S) frame and the F_c frame can then be described by:

$$\begin{bmatrix} a_x^S \\ a_y^S \\ a_z^S \end{bmatrix}_{static} = R_{F_c}^S \begin{bmatrix} 0 \\ 0 \\ -g \end{bmatrix} \quad (5.1)$$

where a^S denotes the accelerations expressed in the sensor frame during the static calibration, and $R_{F_c}^S = R(\phi)R(\theta)R(\psi)$ [46]. The yaw angle (ψ) of the fixture-to-shoe fixture was estimated to be zero

however, the offset could potentially have a different value which will be concluded from the experiments (Chapter 7). The offset is currently set to zero degrees, leading to the sensor-to-foot orientation of $R(\phi)R(\theta)R(0)$:

$$\begin{bmatrix} \cos(\phi) & 0 & -\sin(\theta) \\ \sin(\theta)\sin(\phi) & \cos(\phi) & \cos(\theta)\sin(\phi) \\ \sin(\theta)\cos(\phi) & -\sin(\phi) & \cos(\theta)\cos(\phi) \end{bmatrix} \quad (5.2)$$

Substituting 5.2 into 5.1 results in:

$$\begin{bmatrix} a_x^S \\ a_y^S \\ a_z^S \end{bmatrix} = \begin{bmatrix} \sin(\theta) \cdot g \\ -\cos(\theta)\sin(\phi) \cdot g \\ -\cos(\theta)\cos(\phi) \cdot g \end{bmatrix} \quad (5.3)$$

which will result in

$$\theta = \arcsin\left(\frac{a_x^S}{g}\right) \quad (5.4)$$

$$\phi = \arctan\left(\frac{a_y^S}{a_z^S}\right) \quad (5.5)$$

After evaluation of the fixture concept, the yaw angle (ψ) can be set to an angle describing the offset of the fixture (α_{offset}), illustrated in Figure 2.1.

Foot Progression Angle Estimation

6.1. Stance Phase Detection

The stance phase is the period in the gait cycle when the foot makes contact with the ground, resulting in near-zero foot velocity (Figure 6.1). To isolate this phase, a zero-velocity detection method was adopted [38], previously implemented by Wouda et al. (2021) [33]. This technique entails the fulfilment of four specified conditions, thereby confirming the foot's presence in the mid-stance phase, as listed below:

1. The norm of the acceleration ($\sqrt{a_x^2 + a_y^2 + a_z^2}$) vector must be between 9.0 and 11.0 m/s².
2. The local variance of the acceleration must be below 3 m/s², where the local variance and local mean are defined by:

$$\sigma^2 = \frac{1}{2s+1} \sum_{j=t-s}^{t+s} (a_j - \bar{a}_j)^2 \quad (6.1)$$

With the local acceleration (\bar{a}_j):

$$\bar{a}_j = \frac{1}{2s+1} \sum_{j=t-s}^{t+s} a_j \quad (6.2)$$

Where t is the current time sample, j is the range over which the local variance and mean are determined from $t-s$ to $t+s$, where s is set to an experimentally determined value of $s=3$, resulting in a time period of 0.1167 seconds.

3. The norm of the angular velocities ($\sqrt{\omega_x^2 + \omega_y^2 + \omega_z^2}$) must be below 50 deg/s.
4. The detected mid-stance phase must have at least a duration of 0.167 seconds

The last condition is self-added, to exclude false mid-stance phase detections. With the assumption that during normal walking speed, the mid-stance phase will not be shorter than 0.167 seconds.

Given the constraints of the Xsens DOT's output functionality, it was not possible to directly extract raw acceleration and angular velocity data from the IMU. Nonetheless, it did support the extraction of the variables "dv" and "dq". The "dv" represents the change in velocity, and "dq" represents the change in orientation expressed as a quaternion, both of which are given in a time interval ($dt = 1/freq = 1/60$). The accelerations (a) and angular velocities (ω) were derived from these variables using the following equations:

$$a = \frac{dv}{dt} \quad (6.3)$$

$$\omega = 2 \cdot \frac{dq}{dt} \quad (6.4)$$

Angular velocity is computed as twice the change in quaternion value divided by the time interval. In the formulation of condition 2, it's worth noting that Jimenez et al. (2010) [38] reported that the local variance should exceed the defined threshold. However, this appears to be incorrect as it seems to describe foot activity, rather than a zero-velocity state (See Appendix A). As a result, the conditions set by Wouda et al. (2021)[33] were chosen to be more appropriate for accurate mid-stance phase detection.

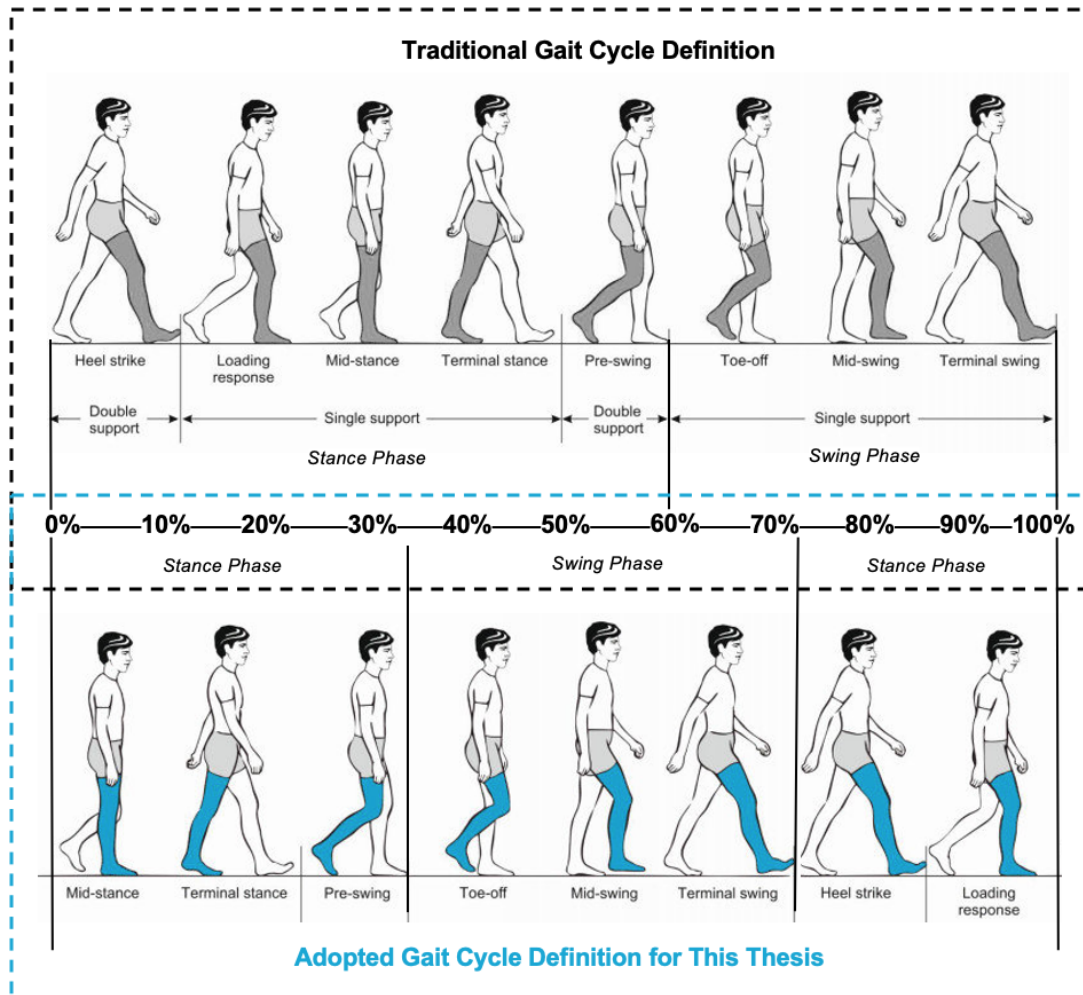


Figure 6.1: Comparison of Traditional Gait Cycle Definition (starting at heel strike and ending at the terminal swing) and the Adopted Gait Cycle Definition used for this thesis starting at mid-stance, as detected by the zero-velocity detection method (Section 6.1), ending during the loading response. The corresponding percentages (%) of each phase within the gait cycle are represented, with the corresponding gait cycle terms.

After the detection of the mid-stance phases, the midpoint of the mid-stance phase was determined as the beginning of the stride, making sure this point was completely in the mid-stance phase. Figure 6.1 shows how the traditional gait cycle definition is transformed into the gait cycle definition within this thesis, where the gait cycle starts (0%) at the middle of the mid-stance phase instead of heel strike. One should note that every gait cycle presented in graphs within this thesis, from now on, uses the Adopted Gait Cycle Definition starting at the middle of the mid-stance phase.

6.2. Orientation Estimation and Transformation of the Accelerations to the Foot Frame

The sensor's output orientation, denoted by quaternions, describes the orientation of the sensor (S) frame relative to the Local Earth-Fixed Reference (L) frame, denoted by the rotation matrix R_S^L . Which is defined by the x-axis directed towards the local magnetic east, the y-axis towards the local magnetic north, and the z-axis upwards.

The orientation of $R_{F_c}^S$ is identified by the calibration method elaborated in section 5.1.4, or by the dynamic calibration method elaborated in section 2.1.1.

The FPA is measured during the mid-stance phase, wherein the velocity approaches zero. Here, orientation estimation drift due to magnetic disturbances can be mitigated using a heading reset. This reset implies that at the beginning of the stride (middle of the mid-stance phase) the L frame is rotated around the z-axis in alignment with the foot's direction at the start of the step (t_0), where the foot is flat on the ground. This defines a new reference frame: the Foot-Flat (F) frame, where it is important to note that this frame is not fixed to the foot, and thus does not rotate with it throughout the remainder of the step. The heading reset results in the rotation matrix R_L^F . Refer to Figure 6.2 for a complete overview of the orientation estimation.

The product of R_L^F and $R_S^L(t)$ gives the rotation matrix $R_S^F(t)$, which is used to rotate the accelerations in the sensor frame (a^S) to the accelerations in the Foot-Flat frame (a^F).

6.3. FPA Estimation

The estimation of FPA from the acceleration in the F frame has previously been executed using two distinct methods by Wouda et al. (2021)[33] and Tan et al. (2021) [32]. One approach involves double integration over the accelerations to obtain the trajectory of the step. Conversely, the other method identifies the point of peak deceleration of the foot during the second half of the swing phase and establishes the FPA from the associated acceleration vector. Within the scope of this thesis, both methodologies are assessed to identify the most accurate means of estimating the FPA.

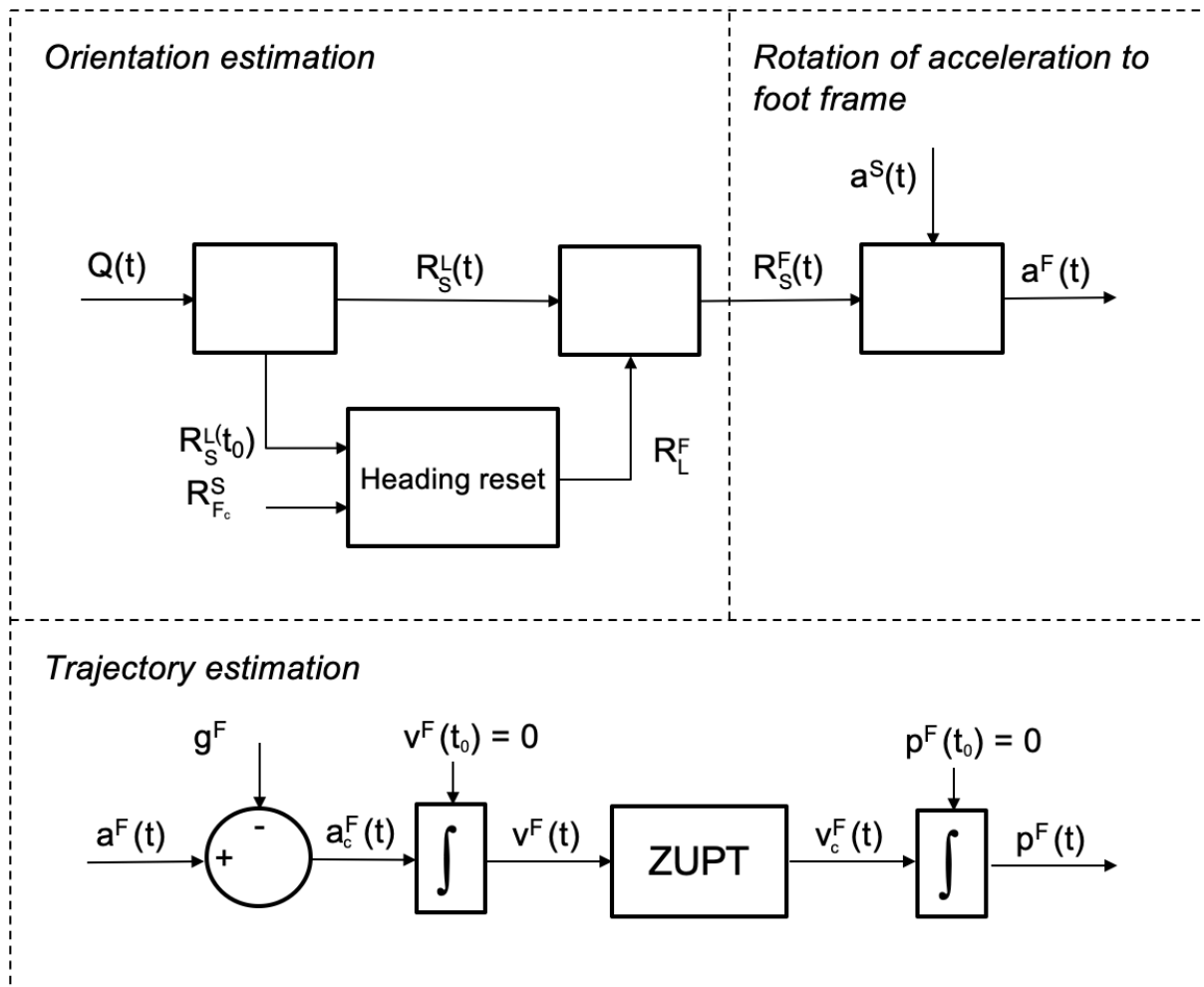


Figure 6.2: Flow chart of the Orientation Estimation including the heading reset, the Rotation of the Accelerations measured within the sensor (S) frame to the Foot-Flat (F) frame and the Trajectory Estimation.

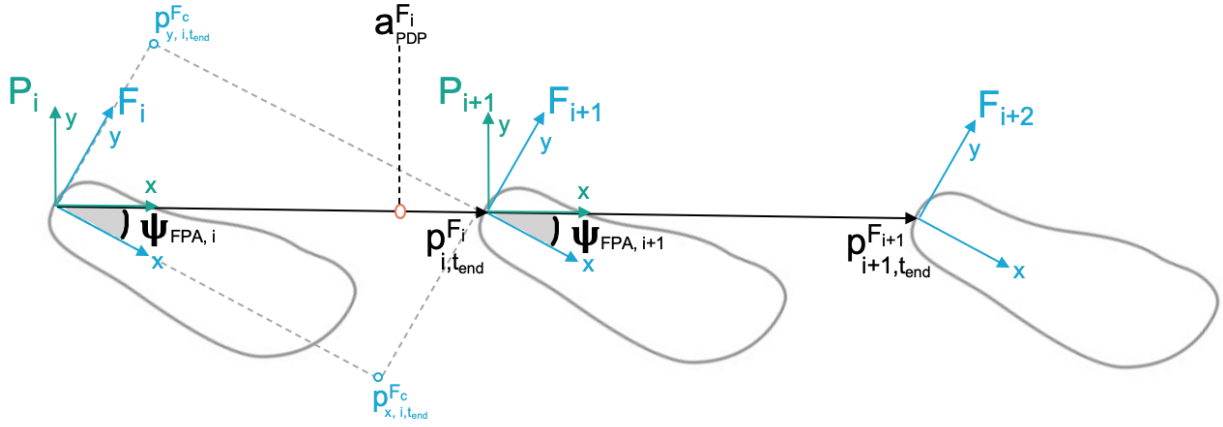


Figure 6.3: Comparison of two methods for Foot Progression Angle (Ψ_{FPA}) estimation of the current stride, denoted by i . Method (1) employs the yaw angle between the Foot-Flat (F) and Progression (P) frames computed from the acceleration during the Peak Deceleration Point ($a_{PDP}^{F_i}$), while Method (2) uses the x and y components of the relative position vector from the stride's beginning ($p_{t_0}^{F_i}$) to its end ($p_{t_{end}}^{F_i}$) in the F frame (i.e., the subsequent mid-stance phase ($i+1$)).

6.3.1. FPA estimation out of the trajectory of the foot

The trajectory of the foot is determined through a process known as strap-down integration [47], which double integrates acceleration data to compute the change in foot position during each stride (Refer to 'Trajectory Estimation' in Figure 6.2). After rotating the acceleration data into the F frame, gravitational acceleration can be eliminated from the data. The accelerations that remain, i.e. free accelerations, are integrated to calculate the foot velocity, starting with an initial velocity $v_{t_0}^F = 0$. Due to the fact that the integration of small biases and noise can lead to drift over time, a zero velocity update is performed to compensate for this drift.

The first part of the zero-velocity update was performed by adjusting all velocities by the initial velocity, v_0 :

$$v'_i = v_i - v_0 \quad (6.5)$$

where i is the current timestep. This ensured that the initial velocity in the updated velocity set v' was zero.

The second part of the zero-velocity update involved linear drift compensation. The total drift (v_D) was calculated as the difference between the final and initial velocities (Δv), divided by the total number of timesteps (i.e. samples) within the stride (N):

$$v_D = \frac{\Delta v}{N} = \frac{v'_{end} - v'_0}{N} \quad (6.6)$$

Then each velocity data point was adjusted to remove the linear drift:

$$v''_i = v'_i - i \cdot v_D \quad (6.7)$$

This ensured that the final velocity v'' had consistent start and end velocities, with the velocities distributed linearly over time.

After obtaining the drift-corrected velocities, another integration stride is performed to obtain the position of the foot with respect to the beginning of the stride, initializing with $p_{t_0}^F = 0$.

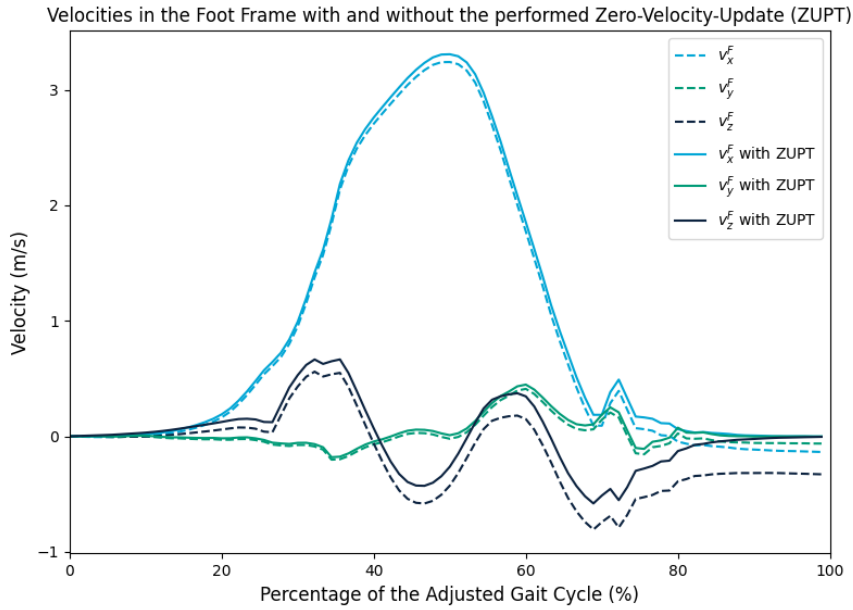


Figure 6.4: The foot velocities (v^F) of one representative participant starting from mid-stance and ending in the next mid-stance (i.e. end of the stride). The foot velocities without the drift compensation of the ZUPT (dashed lines) show an increased velocity in the end of the stride, where the velocities are assumed to be zero.

Because this foot position with respect to the position at the beginning of the stride is determined in the F frame, we know that the angle between the foot vector (x -axis of F frame) and this position vector ($p_{t_{end}}$) is the FPA (Ψ_{FPA}), depicted in figure 6.3). Therefore the FPA of each stride is determined by:

$$FPA = \arctan\left(\frac{p_{t_{end},y}}{p_{t_{end},x}}\right) \quad (6.8)$$

6.3.2. FPA estimation out of the peak deceleration point of the foot

The FPA can be determined exclusively from acceleration data by introducing a new frame, the 'Progression Frame' (P). The x -axis of this P frame aligns with the walking direction (i.e., line of Progression), the z -axis aligns with the gravitational axis, and the y -axis is orthogonal to these axes. Therefore, the rotation from the F to the P frame is defined by the FPA (Ψ_{FPA}), illustrated in figure 6.3:

$$R_S^P = R_F^P R_S^F = R(-\Psi_{FPA}) R_S^F \quad (6.9)$$

where:

$$R(-\Psi_{FPA}) = \begin{bmatrix} \cos(-\Psi_{FPA}) & -\sin(-\Psi_{FPA}) & 0 \\ \sin(-\Psi_{FPA}) & \cos(-\Psi_{FPA}) & 0 \\ 0 & 0 & 1 \end{bmatrix} \quad (6.10)$$

Thus, the accelerations in the Progression frame can be calculated:

$$\begin{bmatrix} a_x^P \\ a_y^P \\ a_z^P \end{bmatrix} = R_F^P \begin{bmatrix} a_x^F \\ a_y^F \\ a_z^F \end{bmatrix} \quad (6.11)$$

Given that the walking direction corresponds to the x-axis in the P frame, the accelerations along the y-axis of the frame are presumed to be zero ($a_y^P = 0$). Substituting this into equation 6.11 results in:

$$\sin(-\Psi_{FPA})a_x^F + \cos(-\Psi_{FPA})a_y^F = 0 \quad (6.12)$$

Hence, the FPA can be determined as:

$$\Psi_{FPA} = \arctan\left(\frac{a_x^F}{a_y^F}\right) \quad (6.13)$$

This method avoids the need for integration and drift compensation over the acceleration data as the FPA can be directly determined. However, the acceleration data at moments of FPA calculation (i.e., during mid-stance phase) is close to zero, which will make it impossible to perform proper FPA estimation from this. As a workaround, the peak deceleration point of the foot during the second half of the swing phase is used, where accelerations exhibit the strongest signal. The limitation of this approach lies in the assumption that the heading direction of the foot from this point to ground contact remains constant, an assumption that may introduce some degree of inaccuracy.

The peak deceleration point of the foot is identified by applying a Hanning window to smooth the acceleration data, with a span size of 0.5 seconds. Within each stride, the mid-stance phase indices, as outlined in 6.1, are excluded. Subsequently, the peak is detected within the second half of the swing phase data, as illustrated in Figure 6.5

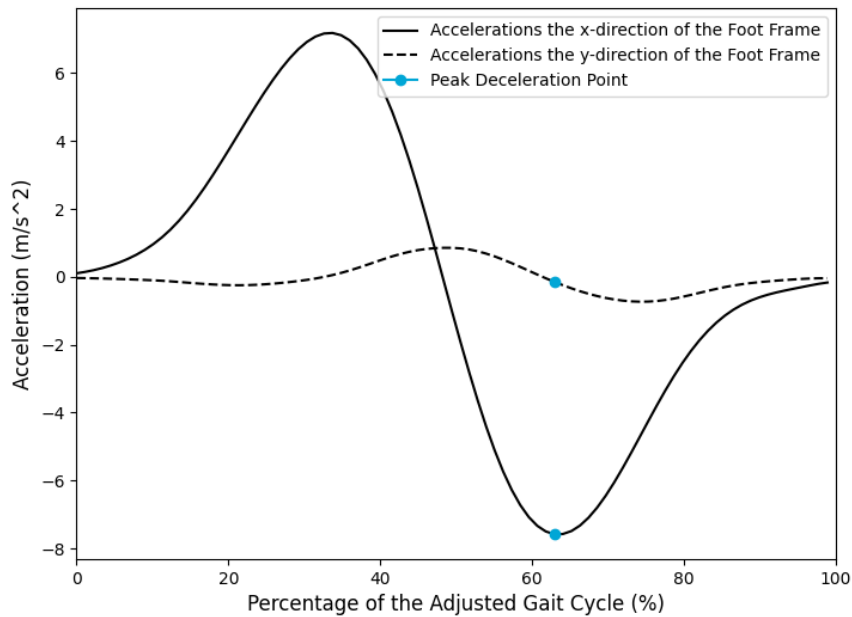


Figure 6.5: The foot accelerations over a representative gait cycle starting at mid-stance (figure 6.1), where the FPA is calculated from the acceleration signals at the peak foot deceleration points (the blue dots), according to equation 6.13, which are detected during the second half of the swing phase.

Experiment Protocol

The experiments involved a total of thirteen participants, consisting of 5 males and 8 females (age: $23,93 \pm 2,16$ years; height: 1.79 ± 0.09 m; weight: 70.95 ± 7.21 kg; body mass index: $22,08 \pm 2,20$ kg/m²). All participants reported no recent injuries that could affect their mobility. Prior to the experiments, the Human Research Ethics Committee (HREC) of the Technical University of Delft reviewed and approved the experiment protocol (Document Number: 2947). Additionally, each subject was required to give their explicit agreement to participate in the study by providing written informed consent. The informed consent document can be found in Appendix G.

The motion trajectories of reflective markers were recorded at a frequency of 100 Hz by the 12 cameras Qualisys optical motion capture system located in the Gait lab of the Biomechanical Engineering Department of the Maritime, Mechanical and Material Engineering (3me) Faculty at the Technical University of Delft. Three reflective markers were attached to the right shoe at the locations: calcaneus, the head of the second metatarsal, and the head of the fifth metatarsal. An additional marker was positioned on the right tibial tubercle. A Qualisys 'small marker cluster' [48] was attached on top of the sensor with markers located on the marker cluster at positions 1, 3 and 4. For the static calibration, four additional reflective markers were secured, one at the apex of the right fibula, one between the first and fifth metatarsal heads of the right shoe, and two on the right lateral and medial malleolus (figure 7.1). Data from the Xsens DOT sensor was recorded at a frequency of 60 Hz, with the output set to Custom Mode 4. This output included orientation data (in quaternions), Kalman-filtered inertial data (dv and dq), and magnetic field readings.

Following a five-second static calibration of both the sensor (Section 5.1.4) and the motion capture system, a dynamic calibration was initiated. Participants were asked to raise their right foot and carry out seven cycles of dorsi- and plantar flexion with their ankles. This activity established the sensor-to-foot orientation from the sensor data (Section 5.1.4). After dynamic calibration, the static markers were removed, initializing the start of the experimental trials.



Figure 7.1: Marker Placement on one of the participants from front, side and back view. And a close-up of the marker placement on the foot of one of the participants, and the sensor with the fixated marker cluster of Qualisys with markers located at positions 1, 3 and 4.

7.1. Experiment 1: Fixture Orientation Following Insertion and Removal from the Shoe

To assess the consistency of the sensor-to-shoe fixture orientation upon multiple fixture attachments on the shoe (subquestion 1 in section 3.2), an experiment was performed where participants were asked to insert and remove the sensor-to-shoe fixture from their right shoe. Participants were specifically asked to wear their own shoes to test the sensor-to-shoe fixture on a variety of shoe types and models. To best simulate the actual application of the fixture, an Xsens DOT sensor without a marker cluster attached to it was used in the sensor-to-shoe fixture. Each participant was permitted a practice attempt, prior to the actual experiment.

The experiment consisted of the participants inserting the fixture into their right shoe and standing on a predefined line in the gait laboratory. The line was parallel to the laboratory's local y-axis and participants were instructed to position their foot directly on the line, which was equivalent to an FPA of around zero degrees (Figure 7.1). Once the participant was properly positioned, the sensor was replaced with another sensor that had the marker cluster attached to it. This was achieved by carefully repositioning the laces that lay over the sensor, moving them above and below the sensor, followed by a sensor swap in the sensor holder (Figure 7.2). With the participant in this alignment, the orientation of both the foot and the sensor was measured for a duration of five seconds using the optical motion capture system. Subsequently, the sensor with the marker cluster was again replaced with the sensor without the marker cluster, and the participant was instructed to remove the fixture. The procedure was repeated twice, resulting in three trials for each participant.

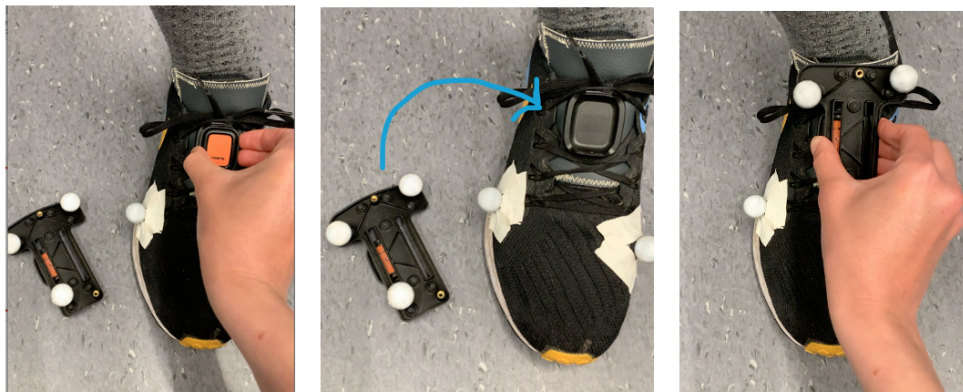


Figure 7.2: Sensor swap of a sensor with and without the attached marker cluster during experiments 1 and 4.

7.2. Experiment 2: FPA Estimation Accuracy of the Algorithms for Normal, Toe-In, and Toe-Out Gait.

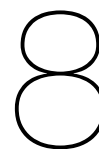
The second experiment aimed to validate the FPA estimation of the proposed algorithm against the optical motion capture system. Each participant performed three trials, one for each walking condition: normal, toe-in, and toe-out. Each trial consisted of the participant walking back and forth along the laboratory walkway four times, covering a total distance of at least 24 meters. Each trial began with the participant lifting their right foot and gently placing it back down. This action helped align the data from the sensor and the motion capture system (Chapter 8).

In preparation for the trials, the sensor with the attached marker cluster was placed in the sensor holder, and the shoelaces were adjusted over the marker cluster to ensure secure placement. The walking conditions were communicated to the participants just before the start of each trial. The sequence of these walking conditions was determined randomly for each participant using an online randomizer tool. Detailed instructions were given to guide the participants on the expected gait patterns. For the natural walking trial, participants were instructed to walk naturally, while attempting to keep their toes pointing forward. In the toe-out and toe-in conditions, participants were asked to point the toes of their right foot outward or inward,

respectively, while walking. The instructions emphasized that these altered FPA's should be performed in a manner and walking speed that was comfortable for the participant. Participants were allowed to practice the walking conditions until they felt confident. Participants received verbal feedback if they failed to maintain the FPA adjustment or over-adjusted the FPA to the point that it clearly impacted other gait parameters, causing unnatural gait patterns.

7.3. Experiment 3: Ten-Minute Walking Trial to Investigate Potential Estimation Drift

The third experiment aimed to validate if magnetic disturbances influenced the FPA estimation over a time period of 10 minutes. An experiment was conducted where participants were asked to walk back and forth on the gait lab's walkway for ten minutes. The walking condition was varied randomly throughout the trial to keep the task engaging for the participants and ensure every walking condition (natural walking, toe-in and toe-out walking) was tested. Each walking condition was performed for 3 to 3.5 minutes, dependent on when the participant was at the end of the walkway. The sequence of the type of walking condition was ordered randomly among participants. Similar to Experiment 2, participants were allowed to perform the walking conditions in a manner and at a walking speed that was comfortable for them and received verbal feedback if needed.



Data Analysis

8.1. Data Processing

All optical motion capture data trajectories were filtered with a low-pass Butterworth filter with a cutoff frequency of 7 Hz. Data points presenting gaps or sudden spikes were disregarded to ensure the integrity of the derived conclusions. Considering the scope of this thesis (Section 1.3), the FPA was only determined during straight-line walking, thus excluding data points corresponding to participant turnarounds on the walkway. This exclusion was based on the following criteria:

- The foot's yaw angle changed more than 45 degrees within a 150-frame window (equivalent to 1.5 seconds).
- The 100 frames (1 second) prior to the 'turning frames' identified in condition 1 were also excluded, as the FPA at the start of the step in these frames depends on the end position in a 'turning frame' and is therefore not reliable within this algorithm.
- The y-values of the marker above the calcaneus fell outside the defined thresholds. The thresholds indicated the area where participants turned (Figure 8.1) and had a maximum and minimum value of 1.5 and -0.6 meters, respectively.

The optical and Xsens DOT data were synchronized by instructing the participants to lift and lower their feet prior to each walking trial (section 7.2). Foot centre accelerations were computed by twice differentiating the trajectories. The first acceleration peak was then identified in both the mocap and IMU data and synchronized. Mid-stance moments, calculated by the proposed FPA estimating algorithm (section 6.1), were converted to the optical frequency of 100 Hz.

As the foot remains stationary throughout the stance phase, perfect alignment between the IMU and mocap indices isn't essential. Nevertheless, the indices must lie within the stance phase. To ensure the transformation from 60 to 100 Hz did not cause mis-synchronisation between the optical and IMU indices, the detected sensor indices were cross-verified against the stance phase recognized by the optical motion capture system by the fulfilment of the same conditions discussed in Section 6.1.

To ensure heading accuracy and hence eliminate drift in orientation data, the sensors must be held still for 2-3 seconds at the start of the measurement [30]. The sensor data was checked to see if the participant stood still for at least 3 seconds prior to lifting the foot; if not, the data file was excluded.

8.2. Sensor-to-Shoe Fixture Validation Calculations

This section details the calculations employed to validate the consistent alignment and stability of the sensor-to-shoe fixture, addressing research question 1. The methodology for determining the difference in FPA estimation accuracy between dynamic and fixture calibration methods is elaborated in section 8.3. The sensor orientation relative to the foot measured by the optical system, denoted as R_F^S , was obtained by multiplying the transpose of the foot orientation ($(R_{LL}^F)^T$) with the sensor orientation (R_{LL}^S) in the lab's local reference frame (LL).

8.2.1. Sensor-to-Shoe Fixture Alignment Post-Attachment

To validate the repeatability of the sensor alignment to the foot (R_F^S) upon repeated attachments, yaw angles were derived from the orientations recorded during each trial of Experiment 1 (Section 7.1). A

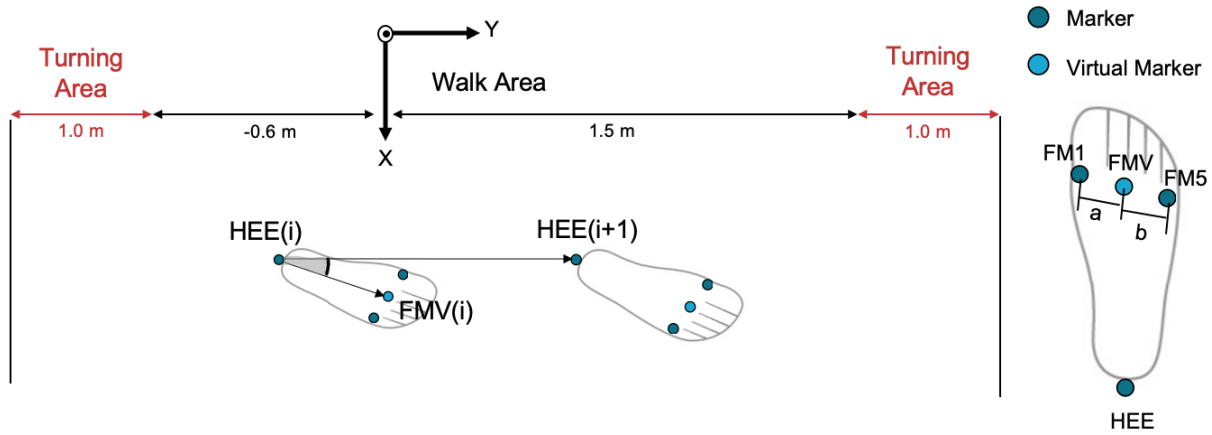


Figure 8.1: Illustration of the optical motion capture lab with the corresponding walkway dimensions and FPA estimation: the angle between the foot vector (FMV(i) - HEE(i)) and the walking vector (HEE(i+1) - HEE(i)). FMV is the virtual marker between the markers above the first and fifth metatarsal head.

Shapiro-Wilk test was then applied to determine the normality of the yaw angle distributions, thereby evaluating alignment consistency.

8.2.2. Sensor stability during walking

To assess the stability of the sensor-to-foot fixture during walking, the R_F^S orientation for the initial 12 steps was calculated and subsequently multiplied by the transpose of the orientation from the trial's first step, providing insight into the relative orientation changes of the sensor-to-shoe fixture from this initial step. Subsequent calculations obtained the Euler angles, from which the mean roll, pitch, and yaw angles at mid-stance for each step across all trials were derived.

8.3. FPA Estimation Algorithm Validation Calculations

This section outlines the calculations employed to validate the FPA estimation algorithm against the optical motion capture system. The accuracy of the algorithm was evaluated by determining the difference between the FPA estimated by the algorithm and the FPA measured by the optical motion capture system. This validation was executed across both algorithms (*Trajectory estimation* and *Peak Deceleration Point*), all walking conditions (*Natural*, *Toe-in*, *Toe-out*), and both calibration methods (*Dynamic* and *Fixture*). To compare the results in the same units as previously published papers that also validated an FPA estimating algorithm, the accuracy of the algorithms was validated with the *Mean Difference*, *Mean Absolute Error (MAE)* and *Root Mean Square Error (RMSE)*.

8.3.1. FPA Calculation from the Trajectories Measured by the Optical Motion Capture System

The FPA measured by the optical motion capture system was calculated from the angle between the measured foot and the walking vector. The foot vector was defined as the line in the horizontal plane from the virtual marker (FMV in Figure 8.1) between the first (FM1) and fifth (FM5) metatarsal head, to the marker above the calcaneus (HEE). The virtual marker's trajectory was formulated as:

$$FMV = \frac{(a \cdot FM5 + b \cdot FM1)}{a + b} \quad (8.1)$$

Here, a and b represent dimensions obtained from the static calibration of the optical motion capture system (Figure 8.1). FPAs with the virtual FMV marker lateral to the calcaneus (HEE marker) were considered positive. The walking vector was defined as the line from the marker above the calcaneus's position at the mid-stance index (i) to the next mid-stance index ($i+1$).

8.3.2. Calculating the Accuracy of the Estimated FPA

To evaluate FPA estimation independently of the sensor-to-foot calibration method accuracy, sensor orientations during static calibration ($(R_S^F)_{static}$), as captured by the optical motion capture system, were employed. This method is further referred to as 'Optical Calibration.' This calibration was used within two distinct algorithms: the Trajectory Estimation and the Peak Deceleration Point algorithm. The fixture and dynamic calibrations were subsequently input into these algorithms to compare their respective accuracies.

For each straight-line walking stride in the trial, the FPA measured by the optical system was subtracted from the FPA estimated by the algorithms, resulting in the difference between the two at each step. Following this, the Mean Difference, MAE, and RMSE values were derived for each trial separately and ultimately the mean and standard deviation were calculated over all trials and participants. The FPA estimation accuracy during the ten-minute walking trials was evaluated by computing the RMSE across all participants every 10 seconds.

8.3.3. Statistical Analysis on the FPA

Two statistical tests were performed to analyse the difference between the FPA measured by the optical and the algorithms and to verify if the optical and algorithms could distinguish the different walking conditions. A significance level of 0.05 was used for both tests.

Paired t-test to verify the difference between optical and algorithm

A paired t-test was employed to assess the significant difference between the FPA measurements from the optical system and the estimates provided by the algorithm. This analysis incorporated data from all trials and participants, segmenting them by the two different algorithms (Peak Deceleration Point and Trajectory Estimation), different walking conditions and calibration methods.

Repeated ANOVA test to verify differences between walking conditions

To ascertain whether the optical system and the algorithms could distinguish differences between the three distinct walking conditions, a repeated measures ANOVA was performed. This test was conducted for both the optical system and the two algorithms, in combination with all calibration methods (optical, dynamic, and fixture), resulting in a total of 7 ANOVA tests.

Part III

Results

Orientation of the Sensor-to-Shoe Fixture to the foot

9.1. Sensor Alignment to the Foot After Repeated Attachments to the Shoe

Figure 9.1 presents a histogram displaying the distribution of the sensor's yaw angle relative to the foot over the 30 trials. The vertical axis represents the frequency of occurrence for each angle displayed on the horizontal axis. The Shapiro-Wilk test indicated that the data are normally distributed ($p=0.8449$), however, notable outliers ranged from -10 to 6 degrees. Notably, the negative outliers correspond to participant P7, while the 2 positive outliers correspond to participant P5 and one to participant P12 (Appendix D table D.1). The mean orientation of the sensor relative to the foot, specifically in the yaw angle, is -0.85 ± 3.63 degrees.

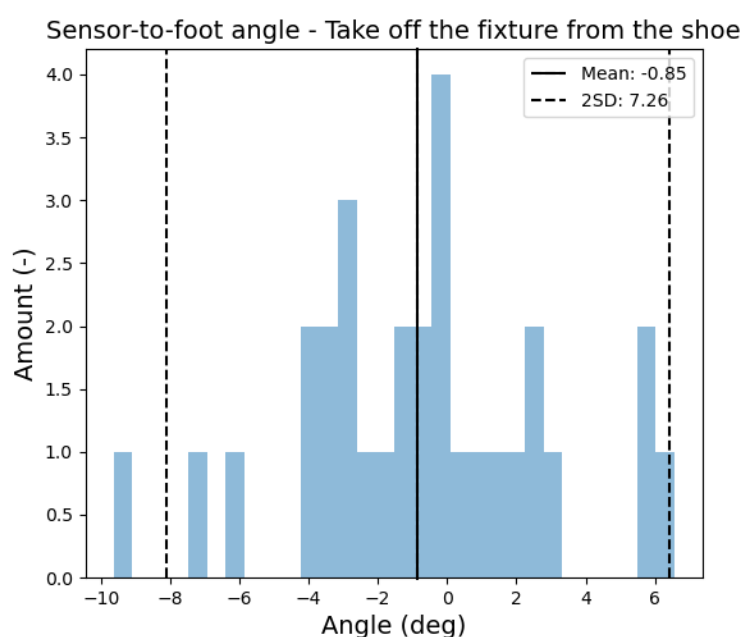


Figure 9.1: Histogram illustrating the distribution of the sensor's yaw angle relative to the foot after removing and reattaching the complete sensor-to-shoe fixture from the shoe, based on 30 trials.

9.2. Sensor Orientation to the Foot During the Three Walking Conditions

Figures 9.2, 9.3, and 9.4 display the average angles of orientation between the sensor and the foot during the Natural, Toe-in, and Toe-out walking trials, respectively. These figures present data from the first 12 steps of each walking trial, with angles measured relative to the orientation in the initial step. In the Natural walking trial, the overall change in yaw, roll, and pitch angles remains around 0 degrees, however, some sudden spikes are observable in the roll and pitch angles.

During the Toe-out and Toe-in walking trials, the change in orientation of the pitch and roll angles remain close to zero degrees, however, the mean yaw angle shifts, decreasing to -1.121 degrees in the Toe-in walking trial and increasing to 0.569 degrees in the Toe-out walking trial after 12 strides.

Table 9.1: The change of the orientation angles in degrees of the sensor to the foot with respect to the first step, during the three different walking conditions.

Roll angle in degrees (Mean±SD)			
Step No.	Natural	Toe-in	Toe-out
1	0 ± 0	0 ± 0	0 ± 0
2	-0,072 ± 1,307	-0,113 ± 0,636	0,137 ± 0,618
3	0,279 ± 1,277	-0,428 ± 1,004	-0,026 ± 0,729
4	-0,389 ± 0,885	-0,084 ± 1,132	-0,036 ± 0,673
5	-0,351 ± 0,815	-0,006 ± 0,763	0,198 ± 0,802
6	0,375 ± 0,971	-0,058 ± 0,683	-0,065 ± 0,602
7	-0,229 ± 1,121	-0,143 ± 0,902	-0,224 ± 1,116
8	-0,061 ± 1,092	0,087 ± 1,311	-0,013 ± 0,991
9	0,124 ± 0,822	-0,37 ± 0,805	0,129 ± 0,925
10	0,096 ± 1,33	-0,289 ± 0,866	-0,087 ± 0,992
11	-0,1 ± 1,097	-0,379 ± 1,016	0,346 ± 0,998
12	-0,658 ± 1,36	-0,076 ± 1,134	-0,023 ± 1,143
Pitch angle in degrees (Mean±SD)			
Step No.	Natural	Toe-in	Toe-out
1	0 ± 0	0 ± 0	0 ± 0
2	0,225 ± 1,23	-0,023 ± 0,903	-0,034 ± 0,475
3	-0,101 ± 1,811	0,089 ± 1,263	-0,228 ± 0,863
4	0,37 ± 1,251	0,334 ± 1,29	-0,004 ± 0,614
5	0,243 ± 1,194	0,232 ± 1,221	0,097 ± 0,757
6	-0,152 ± 0,961	0,295 ± 0,824	-0,617 ± 1,176
7	0,234 ± 1,321	0,078 ± 1,268	-0,059 ± 1,004
8	0,362 ± 0,989	0,149 ± 1,469	-0,159 ± 0,68
9	0,077 ± 1,239	0,32 ± 1,179	-0,145 ± 1,223
10	-0,432 ± 1,136	0,255 ± 1,094	-0,355 ± 1,02
11	0,689 ± 1,496	0,212 ± 1,294	-0,113 ± 0,921
12	0,379 ± 1,19	0,193 ± 1,352	-0,182 ± 0,993
Yaw angle in degrees (Mean±SD)			
Step No.	Natural	Toe-in	Toe-out
1	0 ± 0	0 ± 0	0 ± 0
2	-0,181 ± 0,71	-0,515 ± 0,705	0,201 ± 0,475
3	-0,385 ± 0,872	-0,626 ± 0,69	0,383 ± 0,622
4	-0,069 ± 0,895	-1,057 ± 1,116	0,517 ± 0,581
5	-0,137 ± 0,765	-0,646 ± 0,783	0,577 ± 0,884
6	-0,482 ± 1,139	-0,98 ± 0,893	0,44 ± 1,034
7	-0,289 ± 0,72	-0,886 ± 1,112	0,573 ± 0,885
8	-0,065 ± 0,913	-1,098 ± 0,868	0,553 ± 0,699
9	-0,351 ± 1,267	-1,024 ± 1,066	0,258 ± 0,951
10	-0,354 ± 0,951	-1,239 ± 1,098	0,732 ± 0,759
11	-0,046 ± 1,13	-0,97 ± 1,061	0,561 ± 0,939
12	-0,11 ± 0,85	-1,121 ± 1,148	0,569 ± 0,909

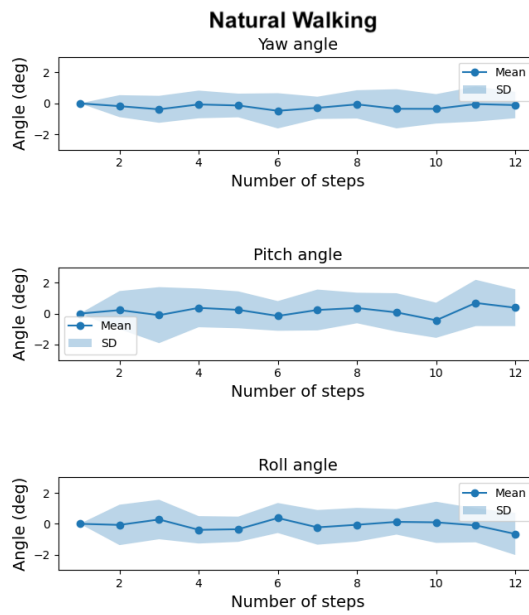


Figure 9.2: The relative change in sensor orientation in relation to the first step, denoting how well the sensor is fixated on the foot during the 'natural walking' trial.

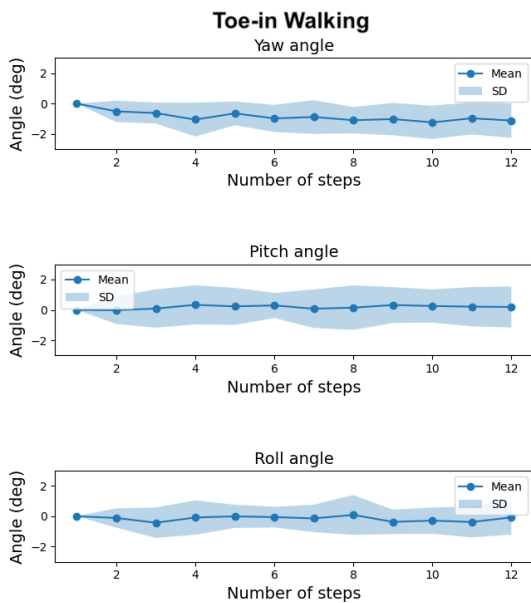


Figure 9.3: The relative change in sensor orientation in relation to the first step, denoting how well the sensor is fixated on the foot during the 'toe-in walking' trial.

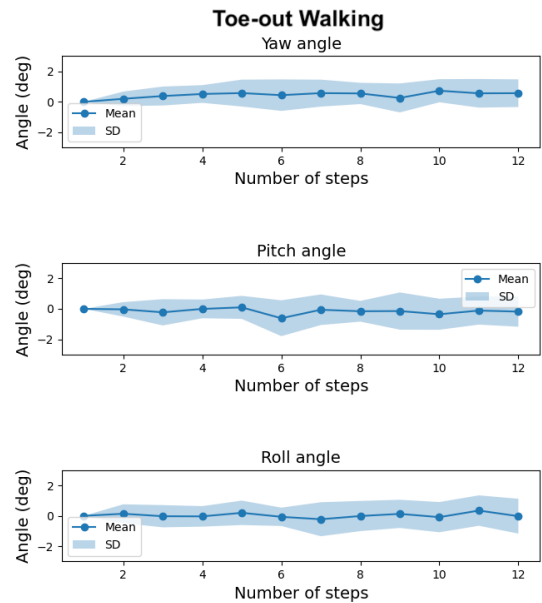


Figure 9.4: The relative change in sensor orientation in relation to the first step, denoting how well the sensor is fixated on the foot during the 'toe-out walking' trial.

Validation of the FPA estimating algorithm

10.1. FPA Estimation by the Two Proposed Algorithms for Three Walking Conditions and Three Different Calibration Methods.

Six files from the dataset were excluded as they started before the participant stood still for three seconds before walking. Additionally, three more files were discarded due to poor marker observation by the optical system, resulting in no representative steps. Moreover, the static recordings for Participants P4 and P12 were lost and consequently excluded. In total, 374, 373, and 409 steps were analyzed for natural, toe-in, and toe-out walking, respectively. In figure 10.1 it can be seen that the overall FPA range during the toe-in walking conditions ranged from -45 to 5 degrees, with an average of -18.22 degrees. For the toe-out walking condition, the overall FPA ranged from 10 to 58 degrees with an average of 31.86 degrees. Participants 1 and 5 showed larger toe-in and toe-out values than all other participants.

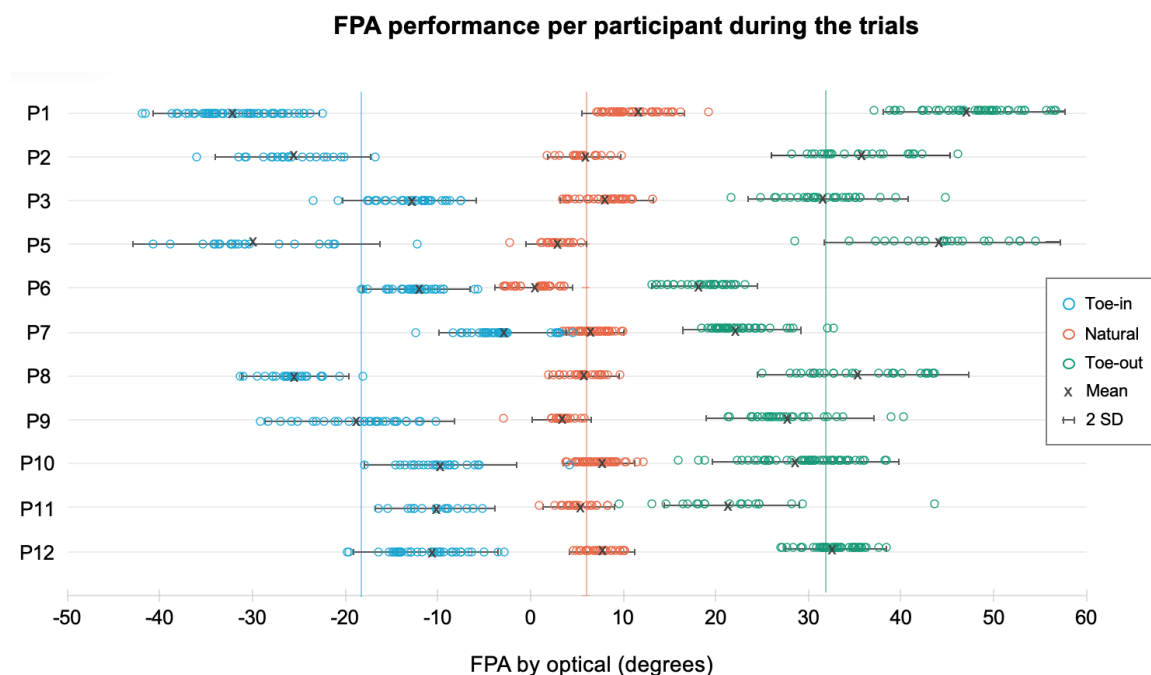


Figure 10.1: FPA values per participant (P) across three walking trials, shown with respective mean and ± 2 SD lines. Average FPA values over all participants for toe-in, natural walking, and toe-out trials were -18.22° (blue line), 6.00° (orange line), and 31.86° (green line), respectively.

In Table 10.1, the Mean Difference, Mean Absolute Error (MAE), and Root Mean Square Error (RMSE) values for both algorithms and various calibration methods are presented. Within the mean difference values, a negative sign indicates undershooting, while a positive sign denotes overshooting. Using the

dynamic calibration method, there was no significant difference in FPA estimation between the algorithms and the optical system, except for the Trajectory Estimating algorithm during natural walking. The optical calibration method showed a significant difference with the peak deceleration point algorithm during natural walking and with the trajectory estimating algorithm for natural and toe-out walking conditions. The mean difference values for both algorithms, when using the optical calibration method, indicate an overshooting estimate. The fixture calibration method indicated a significant difference for both algorithms across all walking conditions, except for the Trajectory estimation algorithm during toe-in walking.

In Figures 10.2, 10.3, and 10.4, a distinct cluster of FPA differences exceeding the 2SD lines is evident with the fixture calibration method, predominantly attributed to Participant P3, as detailed in Appendix E. For the optical calibration method, a similar cluster is observed, lying between the 2SD lines and the mean line for both toe-out and toe-in walking conditions, principally associated with Participants P2, P3, P11 and P13 (Appendix E). Additionally, the figures illustrate a marked increase in random errors between the algorithm’s FPA estimations and the optical system’s measurements, specifically for FPAs greater than 25 degrees and less than -20 degrees.

For the Peak Deceleration Point algorithm, the correlation coefficients (R^2) obtained with the optical, dynamic, and sensor-to-shoe fixture calibration methods are 0.9726, 0.9727, and 0.9711, respectively. Correspondingly, for the Trajectory Estimating algorithm, the (R^2) values are 0.9739, 0.9788, and 0.9722 for the same calibration methods, respectively. The corresponding scatter plots with the correlation coefficients can be found in Appendix D. The repeated measures one-way ANOVA test results indicated that both the algorithms in combination with all calibration methods and the optical system, significantly distinguished between the different walking conditions ($p < 0.001$).

Table 10.1: The mean difference, mean absolute error (MAE) Root Mean Square Error (RMSE) and SD values between the algorithms and the optical motion capture system, for the three difference calibration methods and walking conditions. Bold indicates a significant difference where $p < 0.05$.

Optical Calibration Method								
Walking Condition		Mean diff	SD	MAE	SD	RMSE	SD	p
Peak deceleration point	Natural	1,03	2,89	2,92	1,26	3,16	1,26	<0,0001
	Toe-in	1,43	3,66	3,60	1,63	4,50	1,71	0,1150
	Toe-out	1,18	2,83	3,22	1,16	3,98	1,00	0,0853
Trajectory Estimation	Natural	0,81	3,03	2,92	1,63	3,08	1,60	0,0013
	Toe-in	0,78	3,53	3,18	1,79	3,64	1,90	0,4986
	Toe-out	1,76	3,34	3,69	1,69	4,16	1,44	0,0146
Dynamic Calibration Method								
Walking Condition		Mean diff	SD	MAE	SD	RMSE	SD	p
Peak deceleration point	Natural	-0,40	2,70	2,59	1,14	2,75	1,16	0,0888
	Toe-in	-0,14	3,44	3,36	1,48	4,02	1,64	0,5874
	Toe-out	-0,86	2,76	3,04	0,74	3,85	0,45	0,1897
Trajectory Estimation	Natural	-0,62	2,69	2,51	1,21	2,66	1,23	0,0174
	Toe-in	-0,79	2,97	2,94	1,53	3,19	1,68	0,1536
	Toe-out	-0,29	2,61	2,60	1,03	3,43	0,83	0,5468
Fixture Calibration Method								
Walking Condition		Mean diff	SD	MAE	SD	RMSE	SD	p
Peak deceleration point	Natural	1,97	3,05	2,74	2,20	3,02	2,22	<0,0001
	Toe-in	2,36	3,20	3,43	2,27	4,04	2,30	0,0049
	Toe-out	1,60	2,91	2,98	2,14	3,75	2,03	0,0481
Trajectory Estimation	Natural	1,75	3,07	2,47	2,37	2,67	2,43	<0,0001
	Toe-in	1,71	3,25	3,10	2,21	3,43	2,41	0,0564
	Toe-out	2,17	3,37	3,34	2,57	4,03	2,48	0,0071

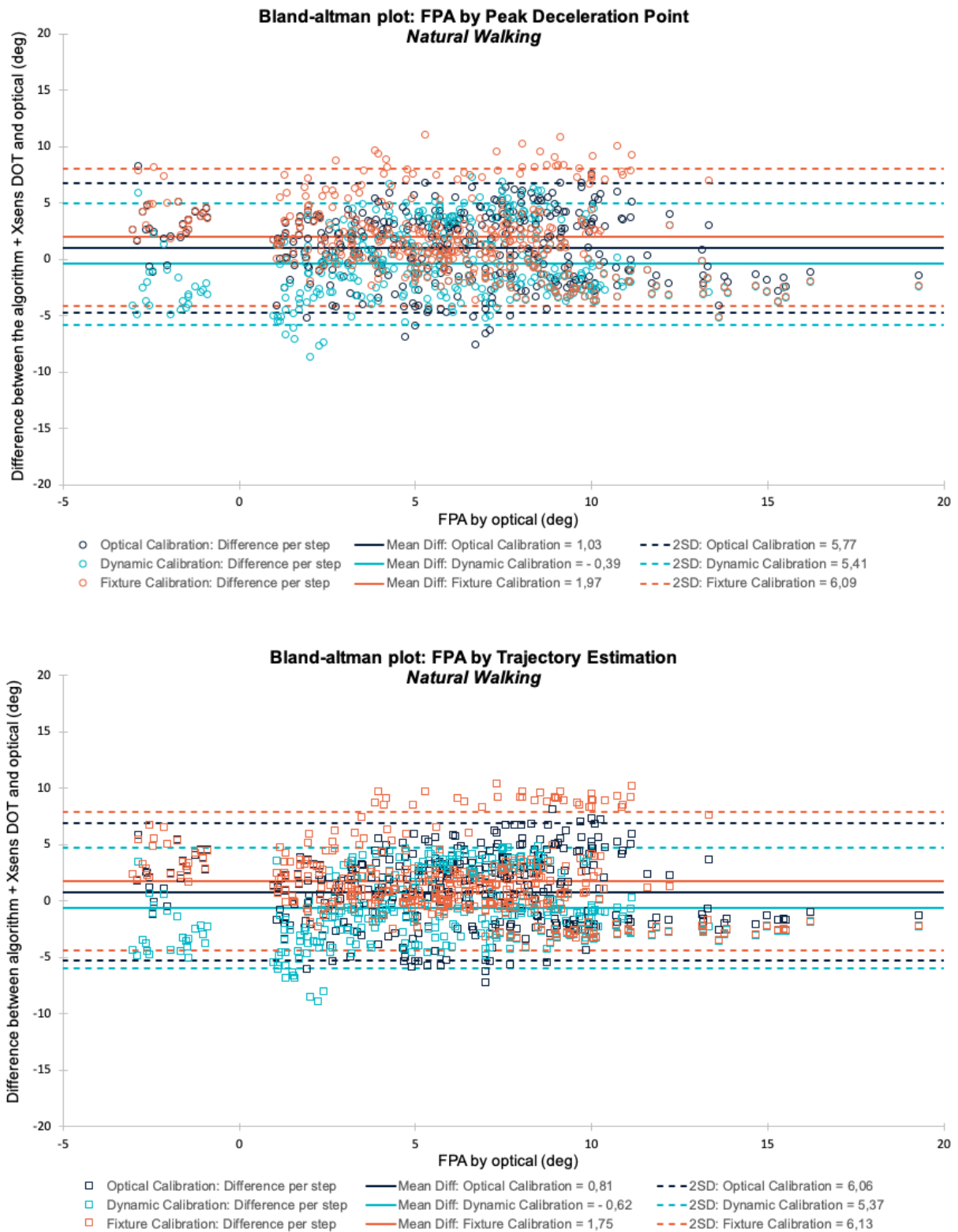


Figure 10.2: The mean difference between the algorithms and the optical system for natural walking, for three different calibration methods: optical (dark blue), dynamic (light blue) and fixture (orange) calibration method. FPA estimating from the Peak Deceleration Point algorithm is shown in the top graph and the FPA estimating from the Trajectory Estimation algorithm is shown in the bottom graph. Each point represents a step.

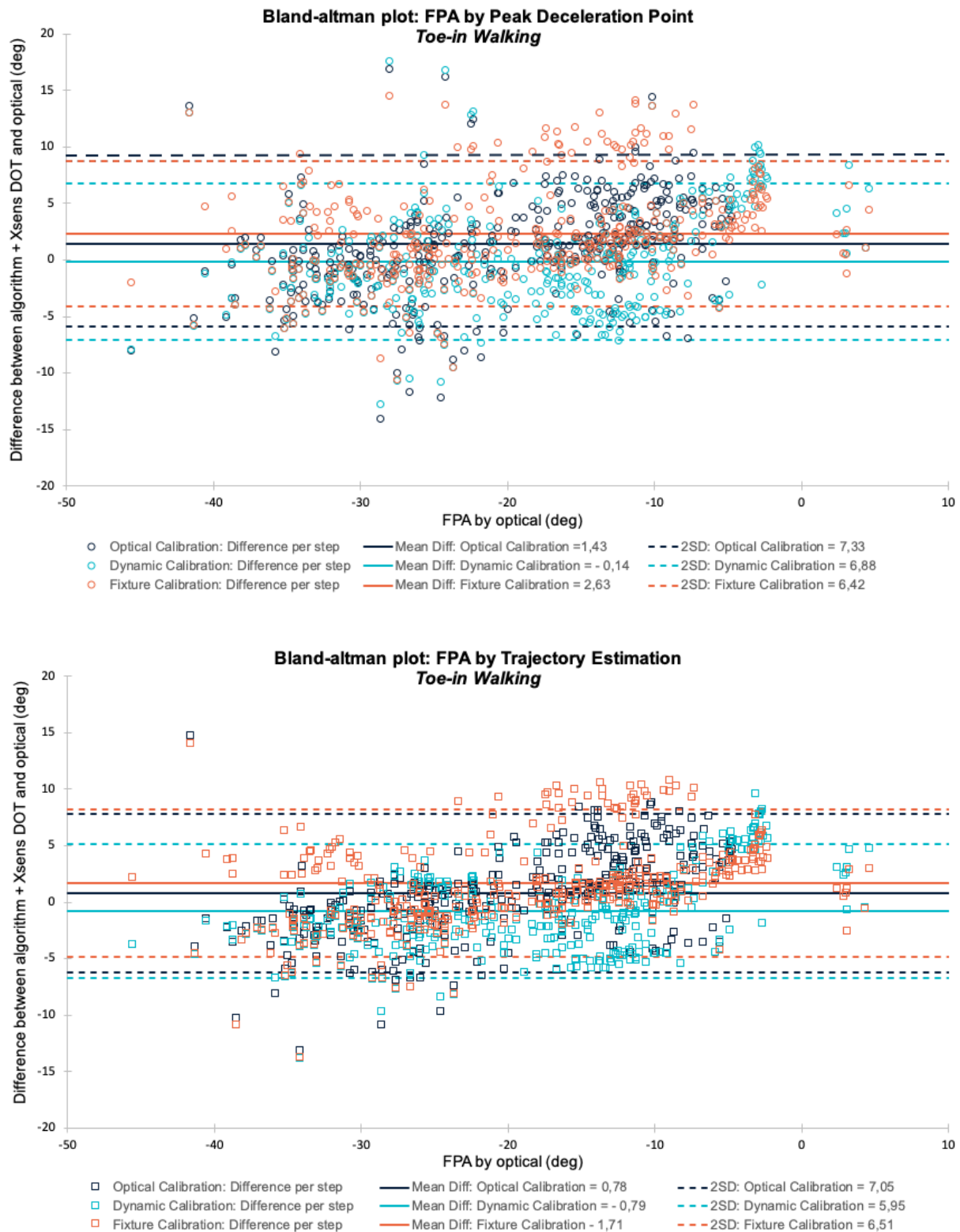


Figure 10.3: The mean difference between the algorithms and the optical system for toe-in walking, for three different calibration methods: optical (dark blue), dynamic (light blue) and fixture (orange) calibration method. FPA estimating from the Peak Deceleration Point algorithm is shown in the top graph and the FPA estimating from the Trajectory Estimation algorithm is shown in the bottom graph. Each point represents a step.



Figure 10.4: The mean difference between the algorithms and the optical system for toe-out walking, for three different calibration methods: optical (dark blue), dynamic (light blue) and fixture (orange) calibration method. FPA estimating from the Peak Deceleration Point algorithm is shown in the top graph and the FPA estimating from the Trajectory Estimation algorithm is shown in the bottom graph. Each point represents a step.

10.2. FPA Estimation over a Period of Ten Minutes

One file was excluded from the dataset of the ten-minute walking trials, as walking started before standing still for three seconds, one extra file was excluded due to poor optical motion capture data resulting in zero representative steps. As discussed before, two participant data's static files were lost and consequently excluded. In total 7 walking files of all around 600 to 650 seconds were analysed resulting in 732 steps.

Figure 10.5 presents the observed Root Mean Squared Error (RMSE) trend over time. It is evident that the RMSE gradually increases with time, with pronounced errors during the 3-5 minute and 6-7.5 minute intervals. These specific intervals correspond to the moment within the experiment when participants transitioned between walking conditions (refer to section 7.3). The Peak Deceleration algorithm demonstrated a lower linear drift (0.0038) over time compared to the Trajectory Estimation (0.005). Despite their distinct initial RMSE values, both algorithms converge to approximately the same RMSE after 10 minutes.

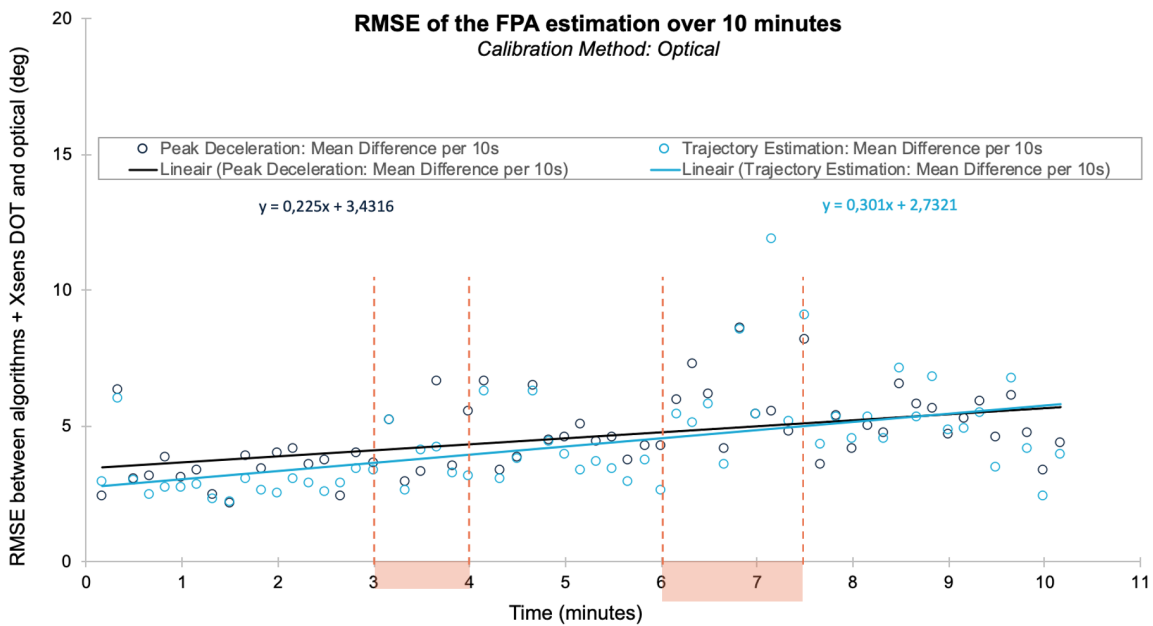


Figure 10.5: The Root Mean Squared Error (RMSE) between the algorithms and the optical reference system over a time period of 10 minutes. Each point represents the RMSE over all trials per 10 seconds. The orange time intervals refer to the moment within the experiment when participants transitioned between walking conditions.

Part IV

Closure

Discussion

11.1. Assessment of the Sensor-to-Shoe Fixture Concept

The assessment of the sensor-to-shoe fixture was conducted through multiple experiments, as detailed in Chapter 7. The focus of the assessment lies on the validation if the fixture indeed maintains a consistent axis alignment along the defined Foot's x-axis, each time it is used. Experiment 1 was designed to evaluate the orientation of the sensor relative to the shoe following the fixture's application. Next to this, Experiment 2 provided data used to assess the stability of this fixture during walking, based on the sensor's orientation to the foot in the initial twelve steps across three walking conditions. The findings of these experiments are discussed herein.

11.1.1. Fixture Stability During Walking Trials

Following from Figure 9.2, 9.3, and 9.4, the fixture remained stable during natural walking trials. However, notable inwards and outwards rotation was observed during toe-in and toe-out walking trials. This rotation may be attributed to momentum forces acting on the fixture during these altered gait patterns. A marker cluster was secured on the sensor (Figure 7.1), and the shoe laces were fastened over this cluster, possibly intensifying the forces exerted on the fixture. Notably, only the first 12 steps were analyzed, making it uncertain whether fixture rotation would continue or stabilize in subsequent steps. Nevertheless, from step 4 onward, the orientation exhibited minimal variation, with changes of approximately 0.6 degrees for toe-out walking and 1.1 degrees for toe-in walking—values that are within an acceptable range.

11.1.2. Fixture Orientation to the Foot After Multiple Attachments to the Shoe

The Shapiro-Wilk test revealed that the angles between the sensor and the shoe followed a normal distribution, with a mean angle of -0.85, suggesting a consistent sensor alignment with the foot. Nonetheless, the presence of pronounced outliers rendered this fixture design unsuitable for FPA estimation. This is because any misalignment of the sensor with the foot along the vertical axis (yaw angle) directly influences the FPA estimation.

Compatibility with different shoe types

During the experiment, Participant P7 experienced challenges attaching the sensor-to-shoe fixture due to the unique design of its shoes. Specifically, the shoe's tongue had its long sides sewn to the shoe body, causing the fixture's width to be incompatible to fit the shoe underneath the laces. As illustrated in Figure 11.1, the sensor-to-shoe fixture for Participant P7 did not align fully with the shoe tongue, complicating the sensor's alignment with the foot. In contrast, as shown in Figure 11.2, the fixture for Participant P4 fit perfectly over the shoe tongue, ensuring a more accurate alignment. These observations indicate that the fixture may not be compatible with all shoe models. However, it's worth noting that shoes with tongues sewn to their sides aren't common, suggesting that such compatibility issues would be rare in the context of the KneeWear feedback device.

Familiarization with the Sensor-to-Shoe Fixture

Participants P5 and P12 did not report fixture placement difficulties during the experiments, however, outliers of 6 degrees were observed. Interestingly, these outliers consistently occurred during the first trials of the experiment. For all participants a subsequent trend towards an orientation angle relative to



Figure 11.1: Participant P7's sensor-to-shoe fixture, showing incomplete alignment with the shoe tongue due to it being sewn to the shoe body, complicating the placement of the fixture.



Figure 11.2: Participant P4's sensor-to-shoe fixture, displaying a complete fit over the shoe tongue which was not sewn to the shoe body, facilitating accurate alignment with the foot.

the foot closer to 0 degrees was noted by the third trial, suggesting a potential benefit from practice or familiarization with the procedure.

User-friendliness of the Sensor-to-Shoe Fixture in comparison to Dynamic Calibration

A challenge observed during the experiments was the difficulty some participants experienced in securing the fixture inside the shoe, describing the attachment process as physically demanding. Considering that the experiments comprised three consecutive trials, this necessitated frequent removal and reapplication of the fixture, which could exacerbate these challenges. However, given that the intended users of the product are likely to be older than the study participants, difficulties in fixture application may be a more pronounced issue for the end users. Consequently, the user-friendliness of this fixture compared to the dynamic calibration method remains questionable.

An additional experiment was conducted to test for improved user-friendliness of the fixture concept. In this setup, participants were asked to take off their shoe while maintaining the fixture inside the shoe, eliminating the need for frequent reattachments of the fixture. The detailed methodology and results of this experiment are provided in Appendix C. Observations revealed that the sensor-to-shoe orientation was randomly distributed among participants, indicating the current fixture design wasn't suited for this approach. However, optimizing the fixture for this approach could greatly enhance user-friendliness. It's worth noting that the dynamic calibration method still requires a fixture for sensor stability on the shoe, reinforcing the need for a user-friendly attachment mechanism and maintaining the need for a sensor-to-shoe fixture.

11.1.3. Sensor-to-Shoe Fixture Calibration Reliance for FPA Estimation in comparison to Dynamic Calibration

In Figures E.3, E.6 and E.9 in Appendix E, Participant P3 consistently showed an approximately 10-degree difference between the algorithms and the optical system utilising the fixture calibration method. Interestingly, Participant P3 exhibited no issues with fixture fixation. In contrast, Participant P7, who experienced fixture fitting issues, did not produce extreme FPA estimation outliers. An explanation for this could be that the negative orientation value of this participant may have compensated for algorithm overshooting estimation, resulting in reduced estimation errors.

Although the histograms exhibit a normal distribution, significant outliers have a substantial impact

on orientation estimations which, in turn, compromises the reliability of the FPA estimation algorithm. As indicated by Table 10.1, there is a notable discrepancy between the FPA estimates derived from this sensor-to-shoe fixture calibration method and those measured by the dynamic calibration method. This contradicts the initial hypothesis that the 'hybrid' fixture calibration method would yield FPA estimations comparable to those obtained through the dynamic calibration method and highlights that this fixture concept was not compatible for accurate FPA estimation.

11.2. Validation of the FPA Estimation Accuracy Utilising the Xsens Dot Orientation Output

Experiment 2, detailed in Chapter 7, evaluated the FPA estimation derived from two distinct algorithms based on the orientation estimation of the Xsens DOT sensor. This experiment encompassed three walking conditions: natural, toe-in, and toe-out. The subsequent analysis employed three calibration methods to assess their respective impacts on the FPA estimation. This section delves into (1) the FPA estimation accuracy utilising the Xsens DOT orientation output, (2) a comparison of the results to prior literature, (3) contrasts the accuracy of the FPA estimation between the Peak Deceleration Point algorithm and the Trajectory Estimating algorithm and (4) discusses the influence of magnetic disturbances on the FPA estimation.

11.2.1. FPA Estimation Performance during Natural, Toe-in and Toe-out Walking

To evaluate the FPA estimation independent of the calibration method accuracy, the optical calibration method was employed as a calibration method (refer to section 8.3.2). The results utilising the optical calibration method showed mean difference values suggesting that the algorithm tends to have an overshooting FPA estimation in comparison to the motion capture system. For all walking conditions, the MAE was below 3.7 degrees. While this doesn't indicate perfect FPA estimation, a deviation of 3.7 degrees is still acceptable for the feedback targets of the proposed feedback device, which are between ± 10 to ± 20 degrees.

Statistical Significance of FPA Estimation Variations Across Walking Conditions

During toe-in walking, the paired t-test showed that the FPA estimation was more precise than during natural and toe-out walking, even though the MAE was lowest for natural walking. This discrepancy might arise from the lower data point variability in the natural walking condition, resulting in greater statistical significance despite the reduced standard error. It remains debatable whether these findings warrant concluding the algorithm is inadequate during natural walking, especially since the significant difference may largely be an artefact of the lower variability. The correlation coefficients across all walking conditions (R^2) were consistently high, exceeding 0.972, indicating strong agreement between the FPAs of the algorithms and the optical motion capture system.

Algorithm Performance Across FPA Ranges

A remarkable pattern observed in the results is the seemingly random algorithm estimations corresponding with larger FPA ranges. As indicated in Figure 10.1, the FPA ranges for participants P1 and P5 significantly exceed those of the other nine participants. Previous studies utilising an FPA feedback program typically reported feedback targets around ± 10 degrees [22, 49, 27, 50]. Therefore, the extreme FPA estimations from participants P1 and P5 may not be representative of how the FPA estimation method will be employed in practice. Excluding all FPA estimations of FPA performance above 45 and below 35 degrees, as detailed in Appendix D Table D.2, the mean difference and MAE error slightly increase with a maximum of 3.81 degrees of MAE utilising the optical calibration method. It should be noted that within the new FPA range of -30 to 40 degrees, the FPA estimation becomes less inconsistent, but remains randomly below -20 and above 25 degrees of FPA. Nevertheless, within the specific use case, when the user is performing extreme FPA an overshooting or undershooting estimation of the algorithm will still make the device provide feedback, which is especially needed at these FPA ranges, therefore this artefact of the algorithm will probably have no outrageous consequences.

Optical calibration method inaccuracies

Higher estimation errors were noted for the optical calibration methods, particularly for Participants P2, P3, P11, and P13, as detailed in Appendix E (see Figures E.1, E.4, E.7). Several factors could explain these

discrepancies when compared to other calibration methods, especially against the dynamic calibration method:

- The sensor-to-shoe orientation might have shifted during the participant's walking trials, making the static calibration's sensor-to-foot orientation unrepresentative, leading to inaccurate FPA estimations.
- The absence of outliers in the results for the dynamic calibration method suggests the sensor orientation may have remained consistent during walking but shifted before the trials. This shift might have occurred during the dynamic calibration (planter-dorsiflexion task), a change captured by the dynamic calibration method but overlooked by the priorly derived optical calibration method during the static calibration.
- A potential error in the optical motion capture system's measurements might have inaccurately determined the sensor-to-foot orientation.

If similar inconsistencies manifest in other participants, they might explain the observed variations between the optical and dynamic calibration methods.

11.2.2. Comparing Xsens DOT Orientation Output to Previous Proposed FPA Estimation Algorithms

Three previous studies have proposed an FPA estimation algorithm employing a single IMU on the foot. This section will compare the accuracy of the Xsens DOT orientation estimation method with the findings presented in these papers. Huang et al. (2016) [31] employed a dynamic calibration method and magnetometer data to correct for orientation estimation drift, reporting average RMSE values for natural, toe-in, and toe-out walking that were approximately one degree lower than the RMSE values obtained in this study (Table 10.1). Wouda et al. (2021) [33], using a magnetometer-free algorithm, reported larger mean differences than our dynamic calibration method combined with the trajectory estimation algorithm (-1.1 ± 3.42 , -0.37 ± 2.8 and 2.4 ± 1.75 for natural, toe-in and toe-out walking respectively). Tan et al. (2021) [32], employing an approach where the sensor was fixated in the shoe, reported Mean Absolute Error (MAE) values close to those obtained with the peak deceleration point algorithm using our optical calibration method, but with comparable errors (2.6 ± 1.1 , 3.8 ± 2.5 and 2.7 ± 1.2 for natural, toe-in and toe-out walking respectively).

FPA estimation averaging over the mid-stance phase

A distinction between this study and Huang et al. (2016) [31] is that the FPA is averaged over the complete stance phase, our proposed algorithm estimates the FPA at the middle of the mid-stance phase. Although foot motion is generally stationary during stance, suggesting FPA may not change substantially, sensor biases could potentially introduce some instability, making averaging over the complete stance phase potentially more reliable.

Impact of varying walking directions during walking

Tan et al. (2021) [32] observed that following a turn during walking, the FPA estimation error was higher for at least seven steps compared to straight-line walking [32]. Notably, both Tan et al. (2021) [32] and Huang et al. (2016) [31] based their examinations on treadmill experiments, only considering the FPA estimation after the initial 20 steps. In contrast, our study used a walkway, with participants walking 4-7 steps, turning, walking 4-7 steps back and turn again, four times per trial. This difference in methodology could explain the difference in FPA estimation error between our algorithm and those proposed by the previous studies. Given the possibility of frequent turns during at-home use of the feedback device, our experimental setup, yielding adequate FPA estimations, appears more comparable with real-life scenarios.

The proposed FPA estimation algorithm is designed exclusively for straight-line walking due to the FPA's non-representative nature during turns, which can be seen in method A of figure 11.3. In daily life, especially at home, turns are frequent which makes recognizing these moments and pausing feedback important.

A published turning detection algorithm correlates well with clinical observations for identifying and evaluating $\geq 90^\circ$ turns among older adults in everyday-life settings [51]. However, even turning angles below 90 degrees can produce non-representative FPA values (Figure 11.3). This highlights that the FPA estimation is really only relevant when walking in a straight line for a longer period of time, for example, at

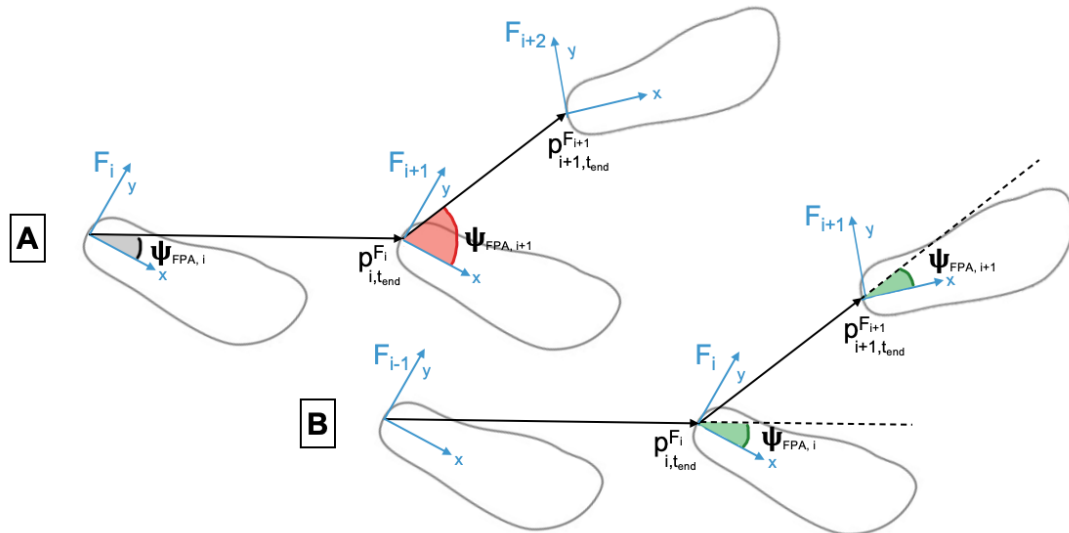


Figure 11.3: Comparison of FPA estimation during turning. Method **A** uses our proposed algorithm, defining FPA as the angle between the foot vector and the subsequent stride's step direction. In contrast, Method **B** defines FPA as the angle between the foot direction and the previous stride's walking direction, aiming to minimize unrepresentative FPAs during turns.

least five steps. It would be more beneficial to detect the walking direction of the previous steps, and when they are within the same range, feedback can start, and if variable, feedback should stop.

Alternatively, redefining the FPA as the angle between the foot direction and the prior step's walking direction may yield more consistent values during turns, as illustrated by Method B in figure 11.3. Noteworthy is that the FPA is officially defined as method A, and also the previous studies that indicated that the FPA is an effective measure to lower the KAM relied on this definition. The effect of the change in the definition of the FPA should therefore be further investigated.

Analysis on the Filtering Methods

Additionally, varying filtering methods are used among the algorithms. Tan et al. (2021) [32] utilized a 0.4-second Hanning window, while the proposed algorithm of this study employs a 0.5-second window, a duration set based on pilot testing. Further analysis could refine this parameter selection.

The hypothesis suggesting that the Xsens DOT orientation estimation method would offer FPA estimation accuracy comparable or superior to magnetometer-free algorithms from prior research is confirmed. The Xsens DOT's estimation appears to outperform the raw gyroscope integration method of Wouda et al. (2021) [33], producing errors similar to those of Tan et al. (2021) [32]. However, the magnetometer-based algorithm of Huang et al. (2016) [31] reported a slightly more accurate FPA estimation, apparent from RMSE values being lower by one degree. This discrepancy might be due to differences between the experimental procedures, with our experimental procedure being more related to the actual use case scenario of the feedback device.

11.2.3. Comparison of Peak Deceleration and Trajectory Estimation Algorithms

Analysis of results from the optical and dynamic calibration methods suggests that the peak deceleration point algorithm slightly outperforms the trajectory estimation algorithm in terms of significance. However, the differences between the errors and correlation coefficients reported by both methods are small and fall within similar ranges, indicating comparable accuracy levels.

FPA estimation for semi real-time feedback provision

Both methods are constrained to estimate the FPA during the stance phase of subsequent steps, delaying feedback until after step completion. Nonetheless, the peak deceleration point algorithm enables FPA estimation just before step completion (i.e. the second half of the swing phase). The accuracy of FPA

estimation by the peak deceleration point suggests that the foot heading direction remains largely consistent after the second half of the swing phase. If this is true for the first half of the swing phase as well, it could permit FPA determination earlier, thereby facilitating more real-time feedback before subsequent FPA adjustments are made, making the peak deceleration point algorithm more suitable for the feedback device [52, 53, 54]. It is important to consider that these assumptions should be rigorously tested on the end-users of the product, as they may exhibit different gait patterns compared to a healthy, younger population without mobility or balance difficulties. Previous research indicates a correlation between these factors and foot heading during the swing phase [55].

The hypothesis declaring that the Trajectory Estimation Algorithm would yield higher accuracy in FPA estimation compared to the Peak Deceleration Point Algorithm is rejected, as both algorithms demonstrated comparable estimation accuracy. Furthermore, the Peak Deceleration Point Algorithm exhibits a greater potential for enabling more real-time algorithm processing and feedback.

11.2.4. Drift in the Orientation Estimation Over Time

The RMSE plotted in Figure 10.5 reveals a noticeable increase in the FPA estimation error over the duration of the 10-minute experiment. This trend is hypothesized to most likely stem from magnetic disturbances affecting the orientation estimation. Drift might be attributed to subtle shifts in the orientation of the sensor-to-shoe fixture, which changed by approximately ± 1 degree after 12 steps, equating to about one-tenth of the steps taken during this experiment (total of 732 steps for 7 participants).

Magnetic Field Considerations within the Gait Lab

The lab environment, crowded with iron objects and electrical devices, was suspected to exert some influence. Although the precise magnetic field conditions within the lab were unknown, Figure 11.4 provides evidence of varying magnetic field strength during the experiment, measured by the Xsens DOT. As indicated by de Vries et al. (2009) [44], such distortions can lead to orientation estimation errors of up to 30 degrees. Upon examining the FPA algorithm's estimation errors after 10 minutes, both the heading reset and XKFcore algorithm appear to counterbalance the impacts of magnetic interference effectively. A further analysis that contrasts FPA estimations with and without the integration of a heading reset in the FPA estimation algorithm could provide a clearer understanding of its actual influence.

Influence of Walking Condition Changes

Notably, there is a marked increase in error during the 3-4 minutes and 6-7.5 minutes intervals. These periods overlap with when participants transitioned between walking conditions (natural, toe-in, or toe-out). This makes it possible that this error could potentially be related more to changes in walking conditions than to fluctuations in magnetic fields.

The hypothesis that magnetic disturbances will influence the orientation estimation over time when using the Xsens DOT, resulting in less accurate FPA estimation, is supported by the observed results. However, it remains challenging to definitively attribute the observed drift in FPA estimation to specific factors, whether they be magnetic disturbances, changes in walking patterns, or shifts in the orientation of the sensor-to-shoe fixture.

11.3. Study Limitations

Sample population

As previously discussed in Section 11.2.3, a significant limitation of this study is the small ($n=13$) sample population, which consisted of young individuals reporting no balance or mobility issues. This demographic may not adequately represent the end-user population for the proposed feedback device utilising this algorithm. Individuals with KOA, who are often older than 50, commonly experience pain and discomfort while walking, leading to different gait dynamics than those observed in a healthy population. It is plausible that not only the FPA estimation may be less accurate for this group, but that altered gait dynamics may also lead to inaccurate stance phase detection. However, a recent study showed promising results for FPA monitoring during daily-life activity in people with and without KOA [21, 56].

Reference data of the motion capture system and its limitations

Another noteworthy limitation was the limited prior experience with the optical motion capture system. Proper placement of markers on participants and effective data collection generally requires familiarity with

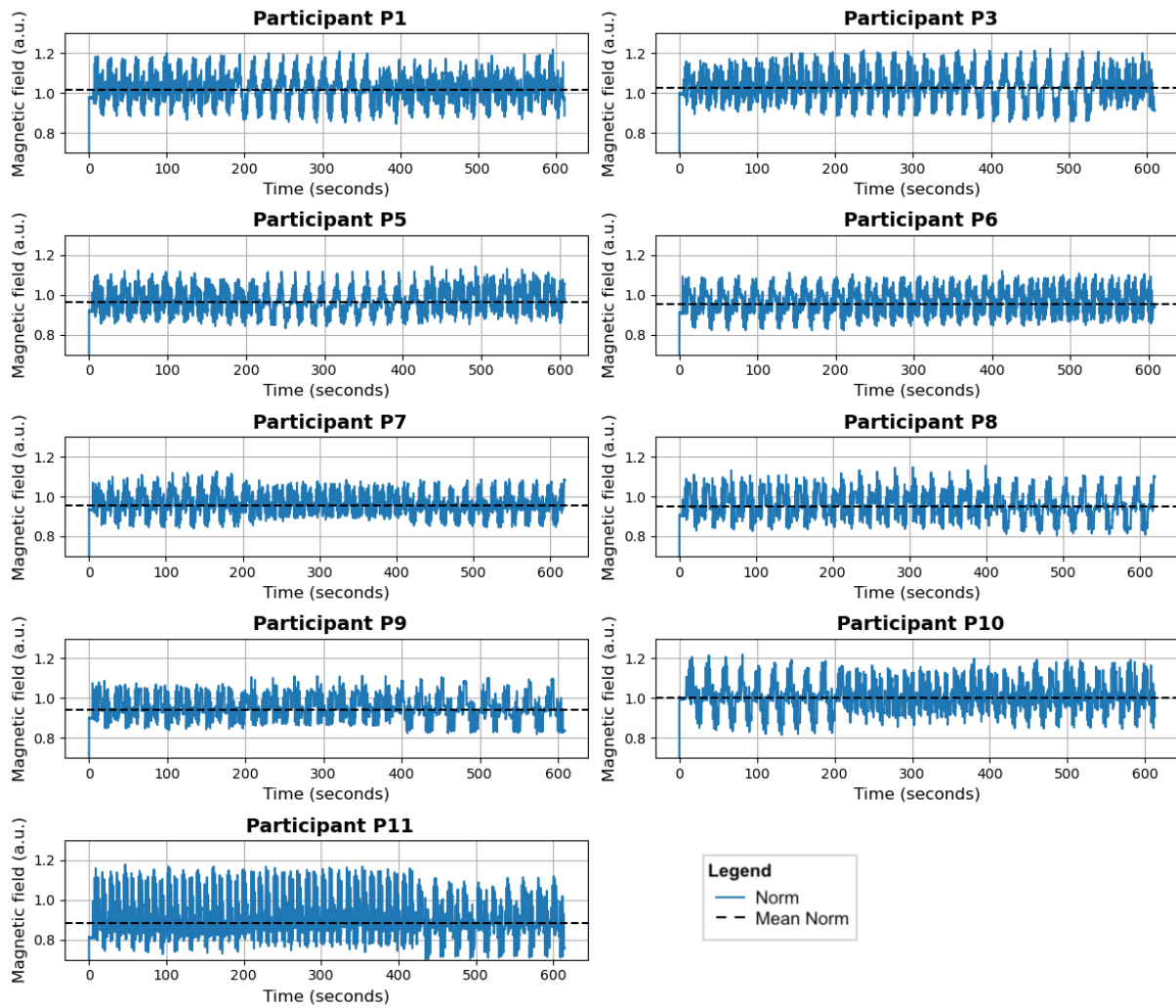


Figure 11.4: The norm of the magnetic field measured by the Xsens DOT during the 10-minute walking trial per participant, including the mean norm value. One a.u. is approximately 40 micro Tesla, as determined at Xsens' calibration lab.

the system. The lack of experience in this study may have led to errors in marker placement or calibration, potentially affecting the accuracy of the motion capture data used for validation.

Moreover, while the FPA was calculated using a virtual marker (FMV), the algorithm was based on foot orientation. A more precise comparison might have been achieved by utilizing the foot orientation derived from FM1, FM5, and HEE (as illustrated in Figure 8.1) rather than the vector between HEE and FMV. This difference is additionally critical since FMV was positioned on the shoe's centre rather than directly on the foot. Additionally, placing the markers on the shoe instead of the foot did not only complicate the precise placement of the markers on anatomical landmarks but also potentially introduces errors based on the assumption that the foot behaves as a rigid body which may be an assumption that does not hold in practice.

Despite being considered a gold standard in gait analysis, the optical motion capture system, now set as the ground truth in this study, is also prone to imprecision and inaccuracies due to factors such as marker occlusion, reflective marker movement, and inaccuracies in marker tracking algorithms [57, 58]. This can result in differences between the system's measurements and actual participant movements, thus introducing uncertainty in the accuracy of the reference data and consequently, the assessment of the algorithm's performance.

Recommendations

Future research to validate this algorithm should prioritize testing with a distinct population group, specifically individuals with KOA, who represent the end users of the product.

Because the fixture-to-shoe concept did not result in accurate FPA estimations, the dynamic calibration method is advised to use as a calibration method. However, the sensor-toe-shoe fixture can be used for mounting the sensor in the shoe. This fixture could be enhanced by redesigning it for compatibility with various shoe types and by developing a more secure attachment method, such as integration with shoe laces. Additionally, the dynamic calibration was now performed under supervision of the researcher in the gait lab, however, when using the device at home it is questionable how precise the users will follow the dynamic calibration instructions, specially upon multiple uses, questioning the accuracy of the dynamic calibration method for the intended use case. It is therefor strongly advised to improve the sensor-to-shoe fixtures alignment to the foot upon multiple uses, or provide intuitive and easily assessable instructions on the dynamic calibration method on the application located on the phone of the user.

Moreover, the algorithm needs further development to transition from its current virtual real-time functionality to true real-time operation. Currently, the algorithm processes pre-recorded data from the sensor and reads this data sample by sample in a Python environment. Future work should focus on integrating the algorithm into the Moveshelf application (Figure 1.1), allowing for real-time sensor data input.

Improvements to the algorithm could also be made. For example, calculating the average FPA over the entire stance phase may enhance performance. Computational efficiency has not yet been addressed and remains an area for potential refinement. Current constraints limit the algorithm to be only compatible with straight-line walking, which is not representative of real-world conditions. The algorithm should be adapted to recognize when participants turn or curve, with corresponding adjustments made to FPA calculation and feedback provision. Redefining the FPA as the angle between the foot vector and the walking direction of the previous step is also an possibility in the mitigation of the unrepresentative nature of the FPA during turning, however, in this case effects of this redefinition on the FPA and its effect on the reduction of the KAM should be investigated.

Haptic feedback integration is another essential future step. The effectiveness of various feedback parameters should be evaluated, building on findings from previous studies [25, 26, 28, 56]. Feedback could be based on multiple FPA values, such as the most recently computed step or an average over the last five steps. If immediate feedback is prioritized, it may be beneficial to calculate the FPA at the peak acceleration point in the initial half of the swing phase. This adjustment could allow feedback to be provided before the user transitions to the subsequent stance phase, potentially facilitating immediate FPA corrections. However, the accuracy of FPA estimations at this peak acceleration point, as opposed to the peak deceleration point, must be confirmed.

Conclusion

13.1. Reflect on the Research Questions

Research Question 1

How effective is the sensor-to-shoe fixture as a calibration method for an FPA estimating algorithm?

The assessment of the sensor-to-shoe fixture indicates that the fixture maintains reasonable stability during natural walking trials. However, small inwards and outwards rotations of about 1 degree were observed during toe-in and toe-out walking, potentially due to momentum forces. The fixture application process was found to be physically demanding, which may present challenges for the intended older end-users. Although the sensor-to-shoe orientation data exhibited a predominantly normal distribution post-sensor-to-shoe fixture insertion, notable outliers were apparent. These outliers had a pronounced effect on FPA estimation, causing the calibration method considerably less accurate compared to the dynamic calibration, and thus making the calibration method utilising this sensor-to-shoe fixture an unreliable method for the FPA estimation algorithm.

Research Question 2

How accurate is the FPA estimating algorithm utilising the Xsens DOT orientation output compared to an optical motion capture system?

The study assessed FPA estimation algorithms under three different walking conditions, utilizing orientation estimation provided by the Xsens DOT sensor. The algorithm, independent of the calibration method accuracy, resulted in MAE values of around 3.0°, while this accuracy is not absolute, it is accurate enough to provide feedback on the FPA. Results indicate that the dynamic calibration method seems to have a beneficial effect on the FPA estimation accuracy. For larger FPA ranges, the algorithm FPA estimations became more inconsistent, however, this will probably not have a substantial influence on the FPA feedback provision. Comparatively, the peak deceleration point algorithm slightly outperformed the trajectory estimation algorithm in terms of significance and potentially ultimately allowing for earlier and more responsive feedback. A drift in the FPA estimation was observed after 10 minutes of walking, which could be attributed to a variety of factors, including magnetic disturbances, shifts in the orientation of the sensor-to-shoe fixture, or changes in walking conditions, but overall the heading reset seemed to effectively mitigate for magnetic disturbances.

13.2. Closing Remarks

This thesis contributes to the ongoing development of wearable technologies aimed at managing Knee Osteoarthritis. By evaluating the FPA estimation algorithms in combination with a single inertial sensor on the foot, this work aims to identify robust and accurate techniques for real-time feedback to KOA patients. This technology has the potential to enable more effective at-home interventions for KOA patients, reducing healthcare costs and improving patient quality of life through enhanced mobility and reduced pain.

While the proposed fixture calibration method needs refining for foot direction alignment, the proposed FPA algorithm, especially when combined with the dynamic calibration method, provided adequate FPA estimations. Performing a heading reset on the orientation estimation at the beginning of each step effectively mitigated magnetic disturbances within the lab.

Future research should be done on the use of the proposed FPA estimating method by the demographic intended for the FPA feedback device, turns detection or redefining the FPA on the angle between the foot vector and the walking direction of the previous step.

By the development of an FPA estimation algorithm, evaluating multiple calibration method, and validating its accuracy and feasibility, this study is a step towards the “Knee Wear project’s” smart-wearable feedback device, simplifying gait retraining interventions for people with Knee Osteoarthritis.

References

- [1] J. W. P. Michael et al. “The Epidemiology, Etiology, Diagnosis, and Treatment of Osteoarthritis of the Knee”. In: *Deutsches Ärzteblatt international* (Mar. 2010). DOI: 10.3238/arztebl.2010.0152. URL: <http://dx.doi.org/10.3238/arztebl.2010.0152>.
- [2] A. Cui et al. “Global, regional prevalence, incidence and risk factors of knee osteoarthritis in population-based studies”. In: *EClinicalMedicine* 29-30 (2020), p. 100587. DOI: <https://doi.org/10.1016/j.eclinm.2020.100587>. URL: <https://www.sciencedirect.com/science/article/pii/S258953702030331X>.
- [3] D. J. Hunter et al. “Osteoarthritis”. In: *The Lancet* 393.10182 (Apr. 2019), pp. 1745–1759. DOI: 10.1016/s0140-6736(19)30417-9. URL: [http://dx.doi.org/10.1016/s0140-6736\(19\)30417-9](http://dx.doi.org/10.1016/s0140-6736(19)30417-9).
- [4] M. M Kawano et al. “Assessment of quality of life in patients with knee osteoarthritis”. In: *Acta Ortopédica Brasileira* 23.6 (Dec. 2015), pp. 307–310. DOI: 10.1590/1413-785220152306150596. URL: <http://dx.doi.org/10.1590/1413-785220152306150596>.
- [5] R. R. Bannuru et al. “OARSI guidelines for the non-surgical management of knee, hip, and polyarticular osteoarthritis”. In: *Osteoarthritis and Cartilage* 27.11 (2019), pp. 1578–1589. DOI: <https://doi.org/10.1016/j.joca.2019.06.011>. URL: <https://www.sciencedirect.com/science/article/pii/S1063458419311161>.
- [6] H. S. Kan et al. “Non-surgical treatment of knee osteoarthritis”. In: *Hong Kong Medical Journal* (Mar. 2019). DOI: 10.12809/hkmj187600. URL: <http://dx.doi.org/10.12809/hkmj187600>.
- [7] K. L. Bennell et al. “Higher dynamic medial knee load predicts greater cartilage loss over 12 months in medial knee osteoarthritis”. In: *Annals of the Rheumatic Diseases* 70.10 (July 2011), pp. 1770–1774. DOI: 10.1136/ard.2010.147082.
- [8] T. Miyazaki. “Dynamic load at baseline can predict radiographic disease progression in medial compartment knee osteoarthritis”. In: *Annals of the Rheumatic Diseases* 61.7 (July 2002), pp. 617–622. DOI: 10.1136/ard.61.7.617. URL: <http://dx.doi.org/10.1136/ard.61.7.617>.
- [9] L. Sharma et al. “Knee adduction moment, serum hyaluronan level, and disease severity in medial tibiofemoral osteoarthritis”. English. In: *Arthritis and Rheumatism* 41.7 (1998). Cited By: 547, pp. 1233–1240. URL: www.scopus.com.
- [10] A. Mündermann et al. “In vivo knee loading characteristics during activities of daily living as measured by an instrumented total knee replacement”. In: *Journal of Orthopaedic Research* 26.9 (Sept. 2008), pp. 1167–1172. DOI: 10.1002/jor.20655. URL: <http://dx.doi.org/10.1002/jor.20655>.
- [11] A. H. Chang et al. “External knee adduction and flexion moments during gait and medial tibiofemoral disease progression in knee osteoarthritis”. In: *Osteoarthritis and Cartilage* 23.7 (July 2015), pp. 1099–1106. DOI: 10.1016/j.joca.2015.02.005. URL: <http://dx.doi.org/10.1016/j.joca.2015.02.005>.
- [12] M. D. C. Silva et al. “Effects of neuromuscular gait modification strategies on indicators of knee joint load in people with medial knee osteoarthritis: A systematic review and meta-analysis”. In: 17.9 (Sept. 2022). DOI: 10.1371/journal.pone.0274874. URL: <http://dx.doi.org/10.1371/journal.pone.0274874>.
- [13] M. Simic et al. “Gait modification strategies for altering medial knee joint load: A systematic review”. In: *Arthritis Care & Research* (2010), n/a–n/a. DOI: 10.1002/acr.20380. URL: <http://dx.doi.org/10.1002/acr.20380>.

- [14] S. Wang et al. "How Foot Progression Angle Affects Knee Adduction Moment and Angular Impulse in Patients With and Without Medial Knee Osteoarthritis: A Meta-Analysis". In: *Arthritis Care Res (Hoboken)* 73.12 (2021), pp. 1763–1776. DOI: 10.1002/acr.24420.
- [15] B. W. Lindsey et al. "Feasibility of Wearable Haptic Biofeedback Training for Reducing the Knee Abduction Moment During Overground Walking". In: *J Biomech Eng* 143.4 (2021). DOI: 10.1115/1.4048082.
- [16] M. J. Booij et al. "Effect of walking with a modified gait on activation patterns of the knee spanning muscles in people with medial knee osteoarthritis". In: *Knee* 27.1 (2020), pp. 198–206. DOI: 10.1016/j.knee.2019.10.006.
- [17] M. A. Hunt et al. "Effects of a 10-week toe-out gait modification intervention in people with medial knee osteoarthritis: a pilot, feasibility study". In: *Osteoarthritis Cartilage* 22.7 (2014), pp. 904–11. DOI: 10.1016/j.joca.2014.04.007.
- [18] R. Richards et al. "Gait retraining using real-time feedback in patients with medial knee osteoarthritis: Feasibility and effects of a six-week gait training program". In: *Knee* 25.5 (2018), pp. 814–824. DOI: 10.1016/j.knee.2018.05.014.
- [19] L. K. Caldwell et al. "Effect of specific gait modifications on medial knee loading, metabolic cost and perception of task difficulty". In: *Clinical Biomechanics* 28.6 (July 2013), pp. 649–654. DOI: 10.1016/j.clinbiomech.2013.05.012. URL: <http://dx.doi.org/10.1016/j.clinbiomech.2013.05.012>.
- [20] P. B. Shull et al. "Muscle force modification strategies are not consistent for gait retraining to reduce the knee adduction moment in individuals with knee osteoarthritis". In: *Journal of Biomechanics* 48.12 (Sept. 2015), pp. 3163–3169. DOI: 10.1016/j.jbiomech.2015.07.006. URL: <http://dx.doi.org/10.1016/j.jbiomech.2015.07.006>.
- [21] J. M. Charlton et al. "Ankle Joint and Rearfoot Biomechanics During Toe-In and Toe-Out Walking in People With Medial Compartment Knee Osteoarthritis". In: *Pm r* 11.5 (2019), pp. 503–511. DOI: 10.1016/j.pmrj.2018.08.388.
- [22] M. A. Hunt et al. "Comparison of mirror, raw video, and real-time visual biofeedback for training toe-out gait in individuals with knee osteoarthritis". In: *Arch Phys Med Rehabil* 95.10 (2014), pp. 1912–7. DOI: 10.1016/j.apmr.2014.05.016.
- [23] R. Richards et al. "The learning process of gait retraining using real-time feedback in patients with medial knee osteoarthritis". In: *Gait Posture* 62 (2018), pp. 1–6. DOI: 10.1016/j.gaitpost.2018.02.023.
- [24] M. A. Hunt et al. "Clinical and biomechanical changes following a 4-month toe-out gait modification program for people with medial knee osteoarthritis: a randomized controlled trial". In: *Osteoarthritis and Cartilage* 26.7 (2018), pp. 903–911. DOI: 10.1016/j.joca.2018.04.010.
- [25] H. Xia et al. "Portable, automated foot progression angle gait modification via a proof-of-concept haptic feedback-sensorized shoe". In: *J Biomech* 107 (2020), p. 109789. DOI: 10.1016/j.jbiomech.2020.109789.
- [26] P. B. Shull et al. "Wearable Real-Time Haptic Biofeedback Foot Progression Angle Gait Modification to Assess Short-Term Retention and Cognitive Demand". In: *IEEE Trans Neural Syst Rehabil Eng* 29 (2021), pp. 1858–1865. DOI: 10.1109/tnsre.2021.3110202.
- [27] J. Xu et al. "Configurable, wearable sensing and vibrotactile feedback system for real-time postural balance and gait training: proof-of-concept". In: *J Neuroeng Rehabil* 14.1 (2017), p. 102. DOI: 10.1186/s12984-017-0313-3.
- [28] A. Karatsidis et al. "Validation of wearable visual feedback for retraining foot progression angle using inertial sensors and an augmented reality headset". In: *J Neuroeng Rehabil* 15.1 (2018), p. 78. DOI: 10.1186/s12984-018-0419-2.
- [29] J. M. Charlton et al. "Remotely delivered, individualized, and self-directed gait modification for knee osteoarthritis: A pilot trial". In: *Clinical Biomechanics* 106 (June 2023), p. 105981. DOI: 10.1016/j.clinbiomech.2023.105981. URL: <https://doi.org/10.1016/j.clinbiomech.2023.105981>.

- [30] *Movella DOT | Movella.com*. URL: <https://www.movella.com/products/wearables/movella-dot>.
- [31] Y. Huang et al. "Novel Foot Progression Angle Algorithm Estimation via Foot-Worn, Magneto-Inertial Sensing". In: *IEEE Trans Biomed Eng* 63.11 (2016), pp. 2278–2285. DOI: 10.1109/tbme.2016.2523512.
- [32] T. Tan et al. "Magnetometer-Free, IMU-Based Foot Progression Angle Estimation for Real-Life Walking Conditions". In: *IEEE Trans Neural Syst Rehabil Eng* 29 (2021), pp. 282–289. DOI: 10.1109/tnsre.2020.3047402.
- [33] F. J. Wouda et al. "Foot progression angle estimation using a single foot-worn inertial sensor". In: *J Neuroeng Rehabil* 18.1 (2021), p. 37. DOI: 10.1186/s12984-021-00816-4.
- [34] J. Favre et al. "3D joint rotation measurement using MEMs inertial sensors: Application to the knee joint". In: (Jan. 2006).
- [35] I. Jolliffe. "Principal Component Analysis". In: *International Encyclopedia of Statistical Science*. Ed. by Miodrag Lovric. Berlin, Heidelberg: Springer Berlin Heidelberg, 2011, pp. 1094–1096. DOI: 10.1007/978-3-642-04898-2_455. URL: https://doi.org/10.1007/978-3-642-04898-2_455.
- [36] I. Skog et al. "Zero-Velocity Detection—An Algorithm Evaluation". In: *IEEE Transactions on Biomedical Engineering* 57.11 (2010), pp. 2657–2666. DOI: 10.1109/TBME.2010.2060723.
- [37] A. M. Sabatini. "Quaternion-based strap-down integration method for applications of inertial sensing to gait analysis". In: *Medical and Biological Engineering and Computing* 43.1 (2005), pp. 94–101. DOI: 10.1007/BF02345128. URL: <https://doi.org/10.1007/BF02345128>.
- [38] A. Jiménez et al. "Indoor pedestrian navigation using an INS/EKF framework for yaw drift reduction and a foot-mounted IMU". In: Mar. 2010. DOI: 10.1109/wpnc.2010.5649300. URL: <https://doi.org/10.1109/wpnc.2010.5649300>.
- [39] P. Felix et al. "ADAPTIVE REAL-TIME TOOL FOR HUMAN GAIT EVENT DETECTION USING A WEARABLE GYROSCOPE". In: Oct. 2017, pp. 653–660. DOI: 10.1142/9789813231047_0079.
- [40] E. Hemingway et al. "Perspectives on Euler angle singularities, gimbal lock, and the orthogonality of applied forces and applied moments". In: *Multibody System Dynamics* 44 (Sept. 2018). DOI: 10.1007/s11044-018-9620-0.
- [41] X. Robert-Lachaine et al. "Effect of local magnetic field disturbances on inertial measurement units accuracy". In: *Applied Ergonomics* 63 (2017), pp. 123–132. DOI: 10.1016/j.apergo.2017.04.011.
- [42] D. Roetenberg et al. "Estimating Body Segment Orientation by Applying Inertial and Magnetic Sensing Near Ferromagnetic Materials". In: *IEEE Transactions on Neural Systems and Rehabilitation Engineering* 15.3 (2007), pp. 469–471. DOI: 10.1109/tnsre.2007.903946.
- [43] E. Palermo et al. "Experimental evaluation of indoor magnetic distortion effects on gait analysis performed with wearable inertial sensors". In: *Physiological Measurement* 35.3 (2014), pp. 399–415. DOI: 10.1088/0967-3334/35/3/399.
- [44] W. De Vries et al. "Magnetic distortion in motion labs, implications for validating inertial magnetic sensors". In: *Gait Posture* 29.4 (2009). Magnetic distortion in motion labs, implications for validating inertial magnetic sensors, pp. 535–541.
- [45] J. Doppler et al. "Variability in Foot-Worn Sensor Placement for Activity Recognition". In: Sept. 2009. DOI: 10.1109/iswc.2009.18. URL: <https://doi.org/10.1109/iswc.2009.18>.
- [46] M. Pedley. "Tilt sensing using a three-axis accelerometer". In: *Freescale semiconductor application note 1* (2013), pp. 2012–2013.
- [47] H. M. Schepers et al. "Ambulatory estimation of foot placement during walking using inertial sensors". In: *Journal of Biomechanics* 43.16 (Dec. 2010), pp. 3138–3143. DOI: 10.1016/j.jbiomech.2010.07.039. URL: <https://doi.org/10.1016/j.jbiomech.2010.07.039>.
- [48] *Small cluster*. URL: <https://www.qualisys.com/accessories/marker-accessories/small-cluster/>.

- [49] S. Bennour et al. "A gait retraining system using augmented-reality to modify footprint parameters: Effects on lower-limb sagittal-plane kinematics". In: *J Biomech* 66 (2018), pp. 26–35. DOI: 10.1016/j.jbiomech.2017.10.030.
- [50] S. D. Uhlrich et al. "Subject-specific toe-in or toe-out gait modifications reduce the larger knee adduction moment peak more than a non-personalized approach". In: *J Biomech* 66 (2018), pp. 103–110. DOI: 10.1016/j.jbiomech.2017.11.003.
- [51] M. H. Pham et al. "Algorithm for Turning Detection and Analysis Validated under Home-Like Conditions in Patients with Parkinson's Disease and Older Adults using a 6 Degree-of-Freedom Inertial Measurement Unit at the Lower Back". In: *Frontiers in Neurology* 8 (2017). DOI: 10.3389/fneur.2017.00135.
- [52] P. B. Shull et al. "Toe-in gait reduces the first peak knee adduction moment in patients with medial compartment knee osteoarthritis". In: *J Biomech* 46.1 (2013), pp. 122–8. DOI: 10.1016/j.jbiomech.2012.10.019.
- [53] B. Lindsey et al. "Reductions in peak knee abduction moment in three previously studied gait modification strategies". In: *Knee* 27.1 (2020), pp. 102–110. DOI: 10.1016/j.knee.2019.09.017.
- [54] R. Richards et al. "Gait Retraining With Real-Time Biofeedback to Reduce Knee Adduction Moment: Systematic Review of Effects and Methods Used". In: *Archives of Physical Medicine and Rehabilitation* 98.1 (Jan. 2017), pp. 137–150. DOI: 10.1016/j.apmr.2016.07.006. URL: <http://dx.doi.org/10.1016/j.apmr.2016.07.006>.
- [55] S. Yamashita et al. "Reducing the foot trajectory variabilities during walking through vibratory stimulation of the plantar surface of the foot". In: *Scientific Reports* 11.1 (2021), p. 7125. DOI: 10.1038/s41598-021-86583-7. URL: <https://doi.org/10.1038/s41598-021-86583-7>.
- [56] J. M. Charlton et al. "Multi-day monitoring of foot progression angles during unsupervised, real-world walking in people with and without knee osteoarthritis". In: *Clinical Biomechanics* 105 (2023), p. 105957. DOI: <https://doi.org/10.1016/j.clinbiomech.2023.105957>. URL: <https://www.sciencedirect.com/science/article/pii/S0268003323000888>.
- [57] M. P. Kadaba et al. "Measurement Of Lower Extremity Kinematics During Level Walking". In: *Journal of Orthopaedic Research* 8 (3 1990), pp. 383–392. DOI: 10.1002/jor.1100080310.
- [58] M. Conconi et al. "Quantification of the errors associated with marker occlusion in stereophotogrammetric systems and implications on gait analysis". In: *Journal of Biomechanics* 114 (2021), p. 110162. DOI: <https://doi.org/10.1016/j.jbiomech.2020.110162>. URL: <https://www.sciencedirect.com/science/article/pii/S0021929020305868>.



Mid-Stance Phase detection by Jiménez et al. (2010) and Wouda et al. (2021)

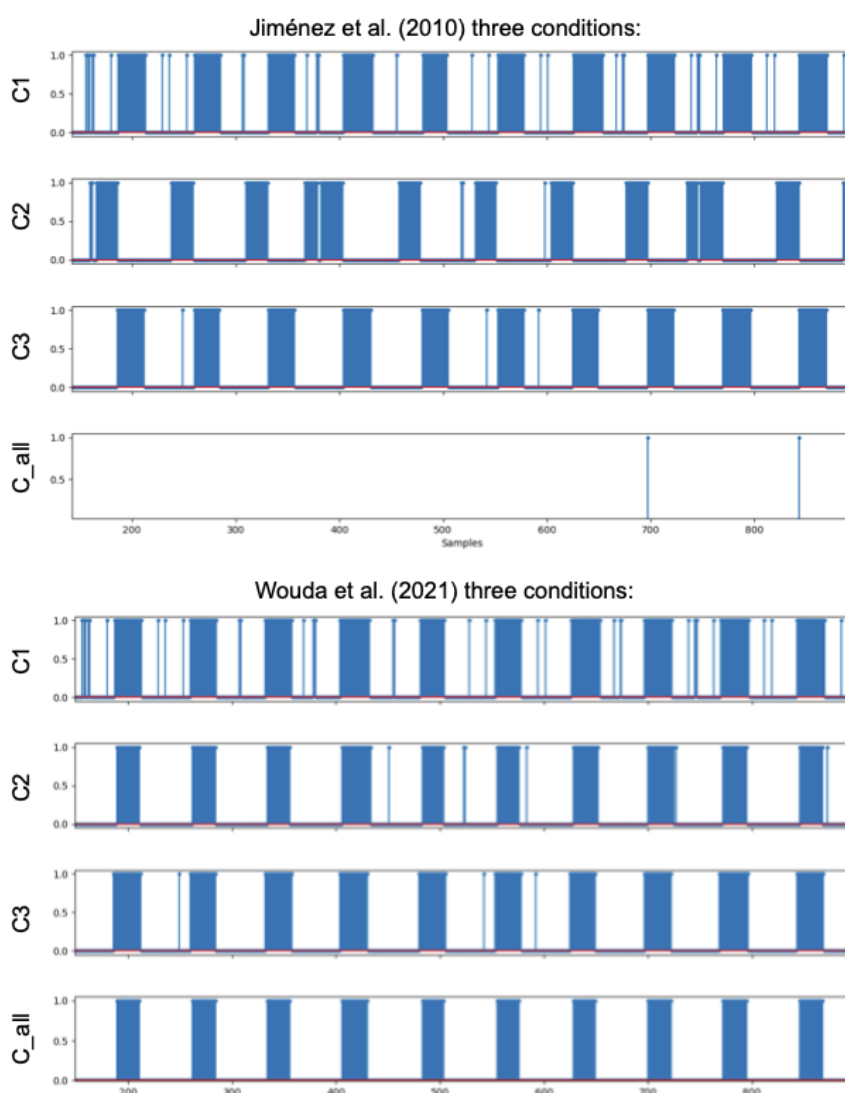
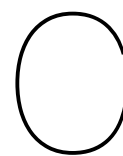


Figure A.1: Comparison of mid-stance phase detection between the studies of Jiménez et al. (2010)[38] and Wouda et al. (2021)[33] under different conditions (C1, C2, C3 and combined C all) as described in chapter 6.1. A value of one signifies that the condition(s) are satisfied, whereas a zero indicates the opposite.



Experiment 4: Assessing the Effect of Keeping the Fixture Inside the Shoe Across Multiple Uses

C.1. Introduction

To enhance the user-friendliness of the sensor-to-shoe fixture concept, this experiment evaluated the impact of leaving the fixture inside the shoe across multiple uses. By doing so, the aim was to alleviate the need for users to attach the fixture each time, simplifying the process and reducing physical effort.

C.2. Methods

Following Experiment 3 (Chapter 7), the sensor with the attached marker cluster was replaced by a sensor without the marker cluster. Ten participants were asked to remove their shoe, leaving the fixture inside (Figure C.1). Upon wearing the shoe again, minor adjustments to the sensor-to-shoe fixture were allowed for proper alignment. The remainder of the experiment followed the same procedures as Experiment 1 (section 7.1), with the sensor's orientation and the foot's orientation being recorded for five seconds. The process was repeated twice more, resulting in a total of three trials per participant.



Figure C.1: Procedure of experiment 4 where the participants were asked to take off their shoe and remain the sensor-to-shoe fixture inside the shoe.

C.2.1. Data Analysis

To validate the repeatability of the sensor alignment to the foot (R_F^S) upon repeated uses while keeping the fixture inside, yaw angles were derived from the orientations recorded by the optical motion capture system during each trial of Experiment 4. A Shapiro-Wilk test ($p < 0.05$) was then applied to determine the normality of the yaw angle distributions, thereby evaluating alignment consistency.

C.3. Results

Figure C.2 presents a histogram of the sensor's yaw angle orientations relative to the foot, after only removing the shoe but leaving the sensor-to-shoe fixture inside. The vertical axis denotes the frequency of occurrence, and the horizontal axis displays the specific angles. Detailed angles for each participant are available in Appendix D Table D.1. A Shapiro-Wilk test suggested the data follows a normal distribution ($p = 0.3721$), however, the distribution appears to be random. The mean yaw angle was -1.58 ± 2.96 degrees, with two pronounced outliers at around -8 degrees attributed to Participant 7.

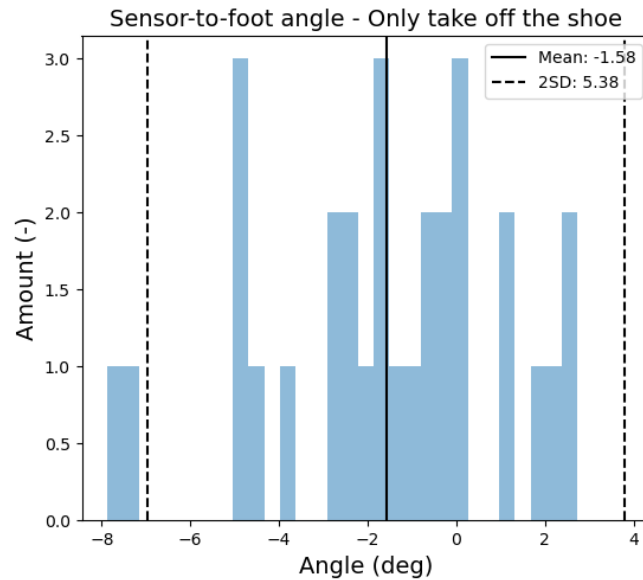
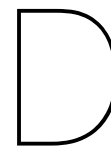


Figure C.2: Histogram illustrating the distribution of the sensor's yaw angle relative to the foot after taking off the shoe while leaving the sensor-to-shoe fixture inside, based on 30 trials.

C.4. Conclusion

While the histogram was identified as a normal distribution, prominent outliers exceeding ± 2 degrees rendered the procedure with this sensor-to-shoe fixture concept unsuitable for consistent sensor alignment to the foot. This is particularly relevant since this sensor's orientation (yaw angle) directly impacts the FPA estimation when using the fixture calibration method. However, for the dynamic calibration method, which could use this sensor-to-shoe fixture to stabilize the sensor on the shoe, the approach is suitable as it allowed the fixture to remain inside the shoe across multiple uses without any of the participants reporting difficulties doing so.



Additional Results

Table D.1: The yaw angle orientation of the sensor to the foot per participant during the experiments where (1) the complete fixture from the shoe was removed, and (2) only the shoe was removed while the fixture was kept inside.

<i>Participant</i>	<i>Trial number</i>	Take off the fixture from the shoe	Take off the shoe
		<i>Yaw orientation angle</i>	<i>Yaw orientation angle</i>
P5	1	6,560246662	-1,620431108
P5	2	5,551930248	2,665503334
P5	3	-3,089338225	-2,136894454
P6	1	2,336195643	-1,494507029
P6	2	-0,410414495	1,316483401
P6	3	0,411438663	0,064350481
P7	1	-9,633581797	-7,464257613
P7	2	-7,33911951	-7,866627699
P7	3	-6,170873623	-7,627699169
P8	1	-1,741104519	-0,3804404
P8	2	-3,776402616	-2,599582301
P8	3	-0,615482161	-3,748990841
P9	1	-3,488900686	-2,77172588
P9	2	-1,133032527	-1,134907603
P9	3	-0,991195379	-4,869335798
P10	1	2,655797026	0,078513898
P10	2	3,096857144	-0,571568777
P10	3	-1,242684555	0,080633979
P11	1	-0,251055374	-1,587631702
P11	2	-2,981459558	-1,634955675
P11	3	2,10030903	-5,012383054
P12	1	5,728364498	-4,537578024
P12	2	-0,292917732	-0,69816378
P12	3	1,19451271	2,302460245
P13	1	-2,441297839	-2,255347632
P13	2	-2,719198335	-4,849373908
P13	3	-4,119201347	-2,22435543
P14	1	-3,629604579	2,022749533
P14	2	1,074225708	0,973153901
P14	3	-0,252154241	-0,315042429

Table D.2: The mean difference, mean absolute error (MAE) and their respective SD values for the FPA performance range between -30 and +45 degrees. Bold indicates a significant difference where $p < 0.05$.

Optical Calibration Method						
	Walking Condition	Mean diff	SD	MAE	SD	p
Peak deceleration point	Natural	1,03	2,89	2,75	1,67	<0,0001
	Toe-in	1,05	3,92	3,84	1,69	0,0037
	Toe-out	0,84	2,64	2,83	1,23	0,0109
Trajectory Estimation	Natural	0,81	3,03	2,70	1,73	0,0013
	Toe-in	0,57	3,57	3,22	1,79	0,0291
	Toe-out	1,52	3,32	3,15	2,02	0,0004
Dynamic Calibration Method						
	Walking Condition	Mean diff	SD	MAE	SD	p
Peak deceleration point	Natural	-0,40	2,70	2,59	1,63	0,0888
	Toe-in	-0,41	3,52	3,40	1,52	0,7420
	Toe-out	-0,95	2,65	2,96	0,86	0,2123
Trajectory Estimation	Natural	-0,62	2,69	2,51	1,55	0,0174
	Toe-in	-0,89	2,92	2,75	1,47	0,2692
	Toe-out	-0,28	2,56	2,41	1,29	0,8378
Fixture Calibration Method						
	Walking Condition	Mean diff	SD	MAE	SD	p
Peak deceleration point	Natural	1,97	3,05	2,89	2,47	<0,0001
	Toe-in	2,06	3,29	3,38	2,25	0,0005
	Toe-out	1,50	2,83	2,85	2,59	0,0058
Trajectory Estimation	Natural	1,75	3,07	2,64	2,53	<0,0001
	Toe-in	1,58	3,14	2,79	2,36	0,0065
	Toe-out	2,18	3,07	3,03	1,96	0,0002

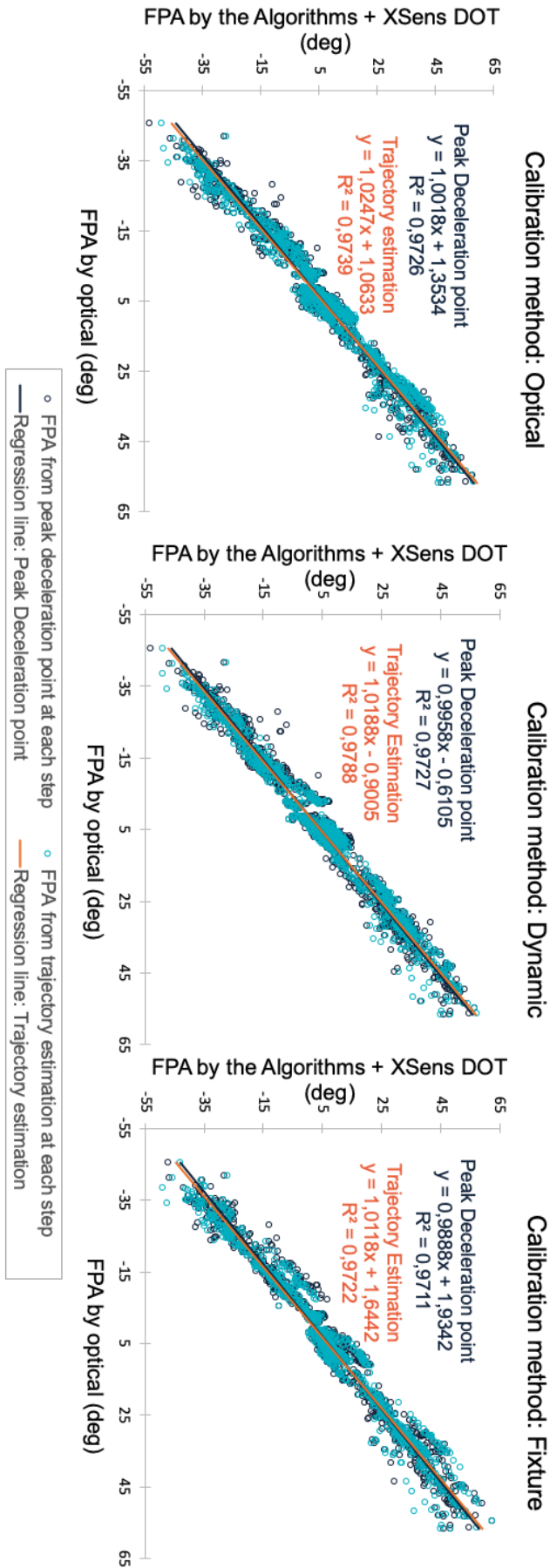
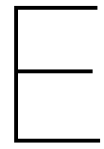


Figure D.1: Scatter plot of each calibration method, showing the FPA estimation of the algorithms compared to the one of the optical system.



FPA Estimation Box-and-Whisker plots

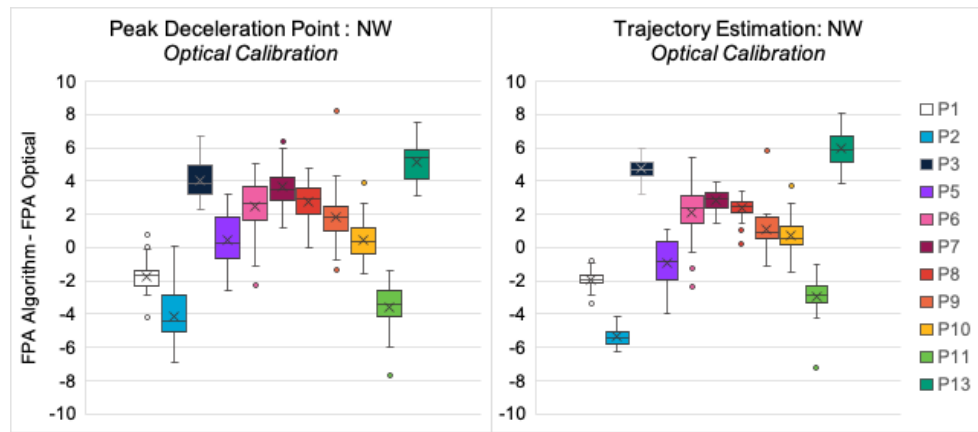


Figure E.1: The Box-Whisker Plots of the difference between the algorithms, Peak Deceleration Point and Trajectory Estimation, and the optical motion capture system of the optical calibration methods and all participants during the Natural (NW) walking trials.

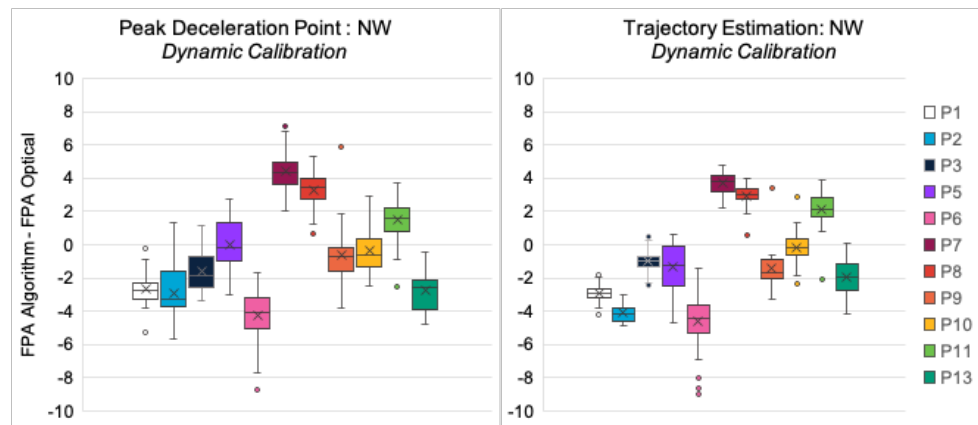


Figure E.2: The Box-Whisker Plots of the difference between the algorithms, Peak Deceleration Point and Trajectory Estimation, and the optical motion capture system of the dynamic calibration methods and all participants during the Natural (NW) walking trials.

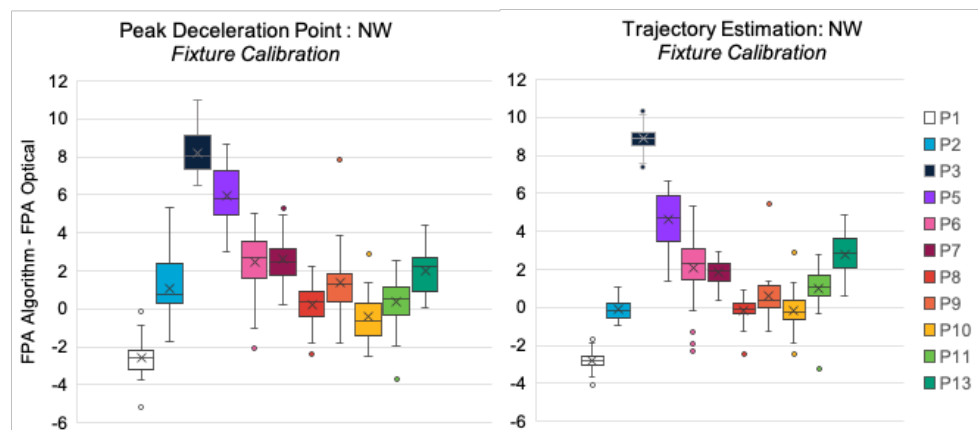


Figure E.3: The Box-Whisker Plots of the difference between the algorithms, Peak Deceleration Point and Trajectory Estimation, and the optical motion capture system of the fixture calibration methods and all participants during the Natural (NW) walking trials.

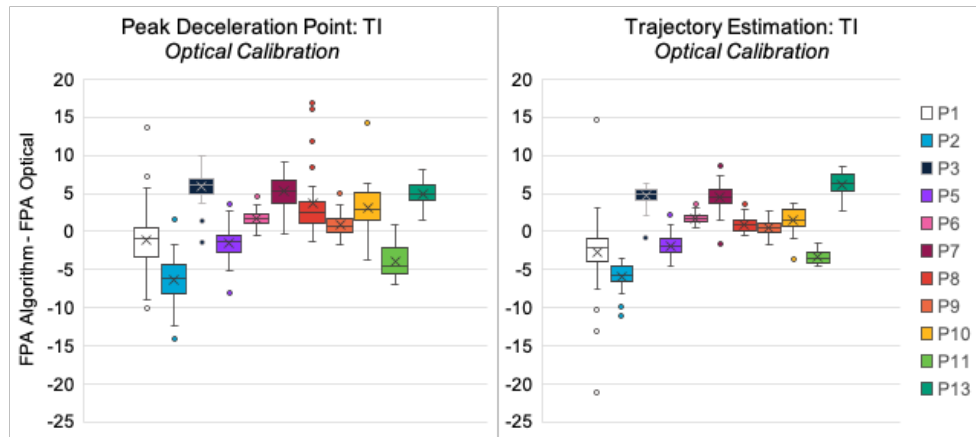


Figure E.4: The Box-Whisker Plots of the difference between the algorithms, Peak Deceleration Point and Trajectory Estimation, and the optical motion capture system of the optical calibration methods and all participants during the Toe-in (TI) walking trials.

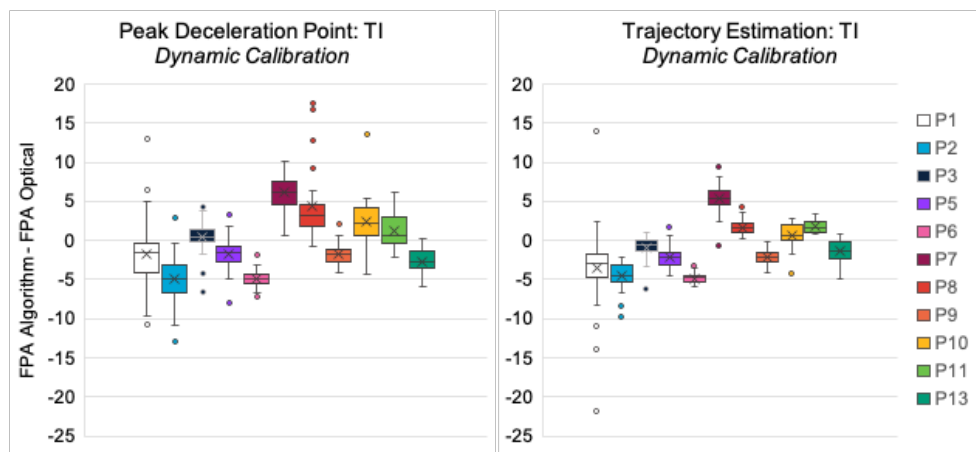


Figure E.5: The Box-Whisker Plots of the difference between the algorithms, Peak Deceleration Point and Trajectory Estimation, and the optical motion capture system of the dynamic calibration methods and all participants during the Toe-in (TI) walking trials.

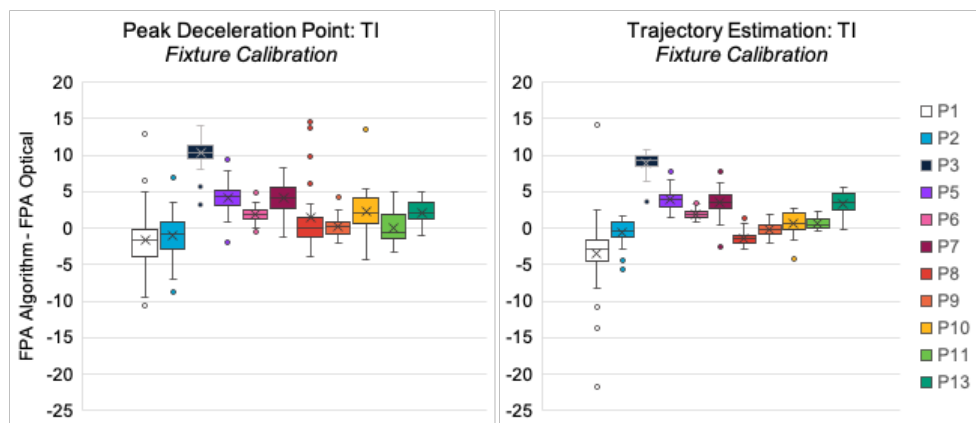


Figure E.6: The Box-Whisker Plots of the difference between the algorithms, Peak Deceleration Point and Trajectory Estimation, and the optical motion capture system of the fixture calibration methods and all participants during the Toe-in (TI) walking trials.

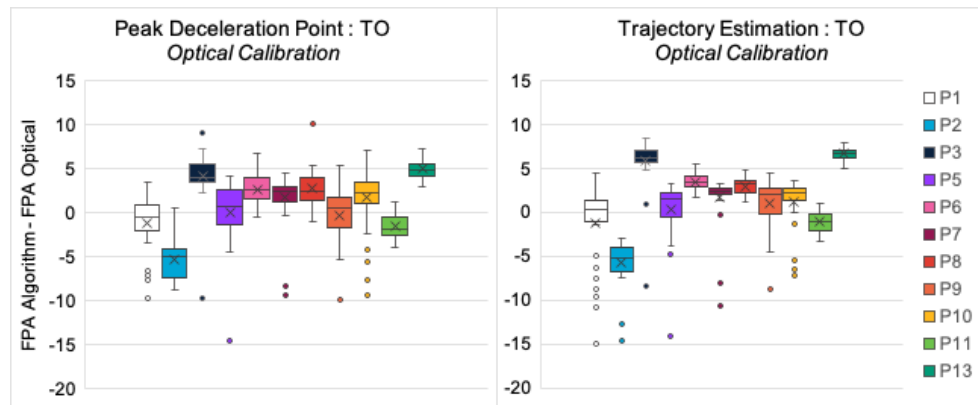


Figure E.7: The Box-Whisker Plots of the difference between the algorithms, Peak Deceleration Point and Trajectory Estimation, and the optical motion capture system of the optical calibration methods and all participants during the Toe-out (TO) walking trials.

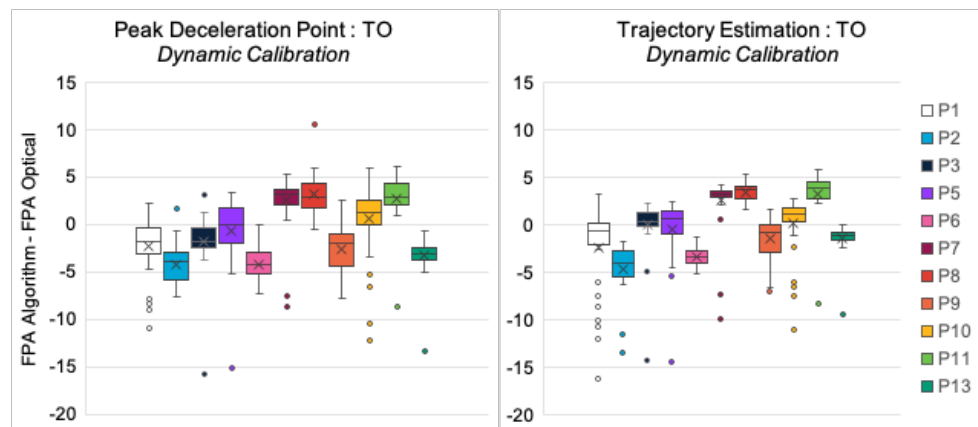


Figure E.8: The Box-Whisker Plots of the difference between the algorithms, Peak Deceleration Point and Trajectory Estimation, and the optical motion capture system of the dynamic calibration methods and all participants during the Toe-out (TO) walking trials.

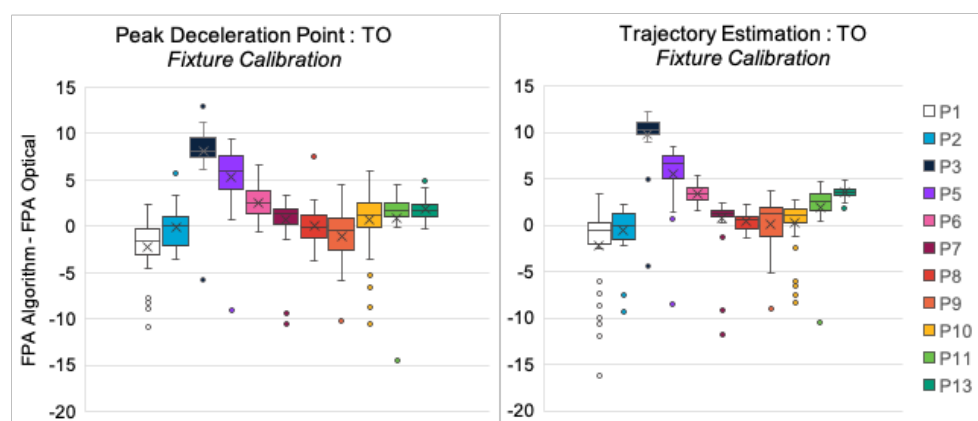
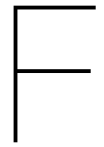


Figure E.9: The Box-Whisker Plots of the difference between the algorithms, Peak Deceleration Point and Trajectory Estimation, and the optical motion capture system of the fixture calibration methods and all participants during the Toe-out (TO) walking trials.



Calibration Set-up of the Optical Motion Capture Lab



Figure F.1: Calibration setup of the Gait Lab of the faculty 3me at the TU Delft. The Qualysis L-frame on the ground serves as the local reference lab frame for this system.

G

Informed Consent Document

Informed consent participation to the research study: “Validation of an FPA feedback prototype.”

Opening statement

You are being invited to participate in a research study titled “Validation of an FPA estimating algorithm”. This study is being done by Floor Heijs, a graduate student from the TU Delft and the graduation internship company Moveshelf.

The purpose of this research study is to validate the accuracy of a Foot Progression Angle (FPA) estimating algorithm using the Xsens DOT which will take you approximately 120 minutes to complete. The data will be used for analysing the accuracy and feasibility of the prototype and the results will be published in the thesis report. We will be asking you to wear and use the FPA feedback prototype during the walking experiments in the Gait lab (dep. BioMechEng., TU Delft).

To the best of our ability your performance in this study will remain confidential. We will minimize any risks by storing the data measured during the experiments on the secured and safe project drive of the TU Delft, to which only the researchers have access. After processing all the data and obtaining the final results, all personal data such as the informed consent forms, and the video recordings will be deleted from the project drive. The anonymized data such as the joint trajectories measured by the sensor and the optical motion capture system of the gait lab will be published publicly on the 4TU.ResearchData repository.

Your participation in this study is entirely voluntary and you can withdraw at any time. You are free to omit any questions. After completing the experiment, you may still request to destroy the data until 26th of May. After this date, the data will be processed within the thesis and therefore data cannot be excluded anymore.

The contact details of the researcher are:

Name: Floor Heijs

Email: floor.heijs@moveshelf.com, or after July 2023: floorheijs@hotmail.com

Phone: 0617280684

PLEASE TICK THE APPROPRIATE BOXES	Yes	No
A: GENERAL AGREEMENT – RESEARCH GOALS, PARTICIPANT TASKS AND VOLUNTARY PARTICIPATION		
1. I have read and understood the study information dated [___/___/___], or it has been read to me. I have been able to ask questions about the study and my questions have been answered to my satisfaction.	<input type="checkbox"/>	<input type="checkbox"/>
2. I consent voluntarily to be a participant in this study and understand that I can refuse to answer questions and I can withdraw from the study at any time, without having to give a reason.	<input type="checkbox"/>	<input type="checkbox"/>
<p>3. I understand that taking part in the study involves: the use of the FPA feedback prototype during a walking experiment in the Gait lab of the TU Delft Department of Biomechanical Engineering. The FPA feedback prototype consists of a sensor-to-shoe fixture on top of my right shoe.</p> <p>A marker-based motion capture system will be recording my foot progression angle (FPA) during walking. The sensor of the FPA feedback prototype will record angular velocities and accelerations which will be the input for the algorithm estimating the FPA. In addition, video recordings will be made of my lower extremity during the walking trials in order to validate the gait events measured by the motion capture system and the sensor. During the study, there will be several trials where different walking conditions will be performed: (1) natural walking, (2) walking with toes pointing outwards (toe-out), and (3) walking with toes pointing inwards (toe-in).</p> <p>Another experiment will be conducted where I will insert and remove the sensor-to-shoe fixture from my shoe several times, to validate what effect this has on the orientation of the sensor relative to the shoe.</p> <p>After the experiments, an analysis will be done on the measured data, determining (1) how accurately the sensor combined with the algorithm can estimate the FPA, relative to the motion capture system and (2) how stable the sensor fixture is and what the orientation is relative to the shoe after insertion and removal.</p> <p>Prior to the experiment, my gender, age, height and weight will be measured and asked, to eventually obtain the average gender, age and BMI among the participants of the research study.</p>	<input type="checkbox"/>	<input type="checkbox"/>
4. I understand that no compensation will be provided for participation in this study.	<input type="checkbox"/>	<input type="checkbox"/>
5. I understand that the study will end as soon as the experiment is over. Which will have approximately a duration time of 120 minutes.	<input type="checkbox"/>	<input type="checkbox"/>
B: POTENTIAL RISKS OF PARTICIPATING (INCLUDING DATA PROTECTION)		
6. I understand that taking part in the study involves the use of the FPA feedback prototype which contains the following risk of the device being a prototype and having no CE certification. I understand that this risk will be mitigated by the approval of the device on safety measurements by the safety officer of 3me. In addition, if any discomfort takes place using the device, it can easily be taken off, and the experiment can be stopped for any reason when desired.	<input type="checkbox"/>	<input type="checkbox"/>
9. I understand that the following steps will be taken to minimise the threat of a data breach and protect my identity in the event of such a breach by saving the data resulting from the experiment	<input type="checkbox"/>	<input type="checkbox"/>

PLEASE TICK THE APPROPRIATE BOXES	Yes	No
<p>on a secure project drive of the TU Delft where identification of the data is not possible because no names of identifiable video recordings will be stored. The informed consent form will also be stored in the project drive, but in a different folder than the measured data which cannot be linked to the measured data. Personal data, containing the video recordings of the lower extremity and the informed consent will be destroyed after the project. Personal data such as my gender, height, weight and age will be stored in an Excel file that cannot be linked to the other data and will only be used to calculate the average gender, age and BMI among the participants of the research study.</p>		
<p>10. I understand that personal information collected about me that can identify me, such as my name, will not be shared beyond the study team.</p>	<input type="checkbox"/>	<input type="checkbox"/>
<p>11. I understand that the (identifiable) personal data I provide will be destroyed after the project, which will be in July 2023.</p>	<input type="checkbox"/>	<input type="checkbox"/>
C: RESEARCH PUBLICATION, DISSEMINATION AND APPLICATION		
<p>12. I understand that after the research study the de-identified information I provide will be used for the results in the thesis report that will be published on the TU repository.</p>	<input type="checkbox"/>	<input type="checkbox"/>
D: (LONGTERM) DATA STORAGE, ACCESS AND REUSE		
<p>16. I give permission for the de-identified sensor output (angular velocities and accelerations) and the FPA angles measured by the optical motion capture system to be archived in 4TU.ResearchData repository so it can be used for future research and learning.</p>	<input type="checkbox"/>	<input type="checkbox"/>
<p>17. I understand that access to this repository is open.</p>	<input type="checkbox"/>	<input type="checkbox"/>